

PORE-SCALE DUAL-DOMAIN FLOW AND TEMPORAL VARIABILITY IN
RECHARGE, HIGH PLAINS AQUIFER, USA

AS
36
2011
GEOL
.E94
v.1

A thesis submitted to the faculty of
San Francisco State University
In partial fulfillment of
The Requirements for
The Degree

Masters of Science
In
Geosciences

By

Brent Corbin Everett

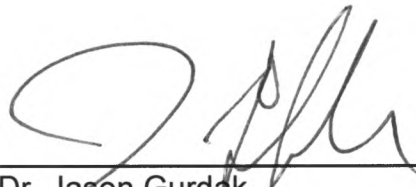
San Francisco, California

May, 2011

Copyright by
Brent Corbin Everett
2011

CERTIFICATION OF APPROVAL

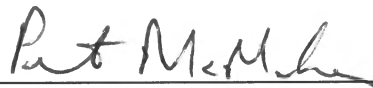
I certify that I have read *Pore-scale dual-domain flow and temporal variability in recharge, High Plains aquifer, USA* by Brent Corbin Everett, and in my opinion this work meets the criteria for approving a thesis submitted in partial fulfillment of the requirements for the degree: Master of Science in Geosciences at San Francisco State University.



Dr. Jason Gurdak
Assistant Professor of Geology



Dr. Leonard Sklar
Assistant Professor of Geology



Dr. Pete McMahon
U.S. Geological Survey

PORE-SCALE DUAL-DOMAIN FLOW AND TEMPORAL VARIABILITY IN
RECHARGE, HIGH PLAINS AQUIFER, USA

Brent Corbin Everett
San Francisco, California
2011

Between 2006 and 2010, heat dissipation probes monitored real-time matric potential at various depths in the vadose zone beneath two semiarid natural grassland sites within the High Plains aquifer. Monitoring results indicate 1) a downward potential for water movement, 2) at least 4 wetting fronts that rapidly propagated to previously unobserved depths (7.3 to 23.0 m below land surface), and 3) rapid water fluxes (0.9 to 6.8 mm/day) that likely resulted in recharge events during the period of observation. Measured water fluxes are orders of magnitude greater than previous estimates using convention tracer-based techniques that provide average water fluxes over decadal to millennial timescales. The rapid water fluxes are likely controlled by pore-scale dual-domain flow. Using observations from this study, I propose a new conceptual model of water flux in the vadose zone beneath natural grasslands in semiarid climates. The model conceptualizes monotonically decreasing total potential, and deep and rapid water movement that can result in episodic recharge events. The movement of water on daily to monthly timescales has important implications for the enhanced mobilization of some fraction of surface-derived contaminants in the vadose zone to groundwater. Most notably, interpretations of the observations and reported water fluxes from this study may account for the inconsistencies between observed groundwater chemistry and previously estimated chemical fluxes in the vadose zone of the High Plains aquifer.

I certify that the Abstract is a correct representation of the content of this thesis.



Chair, Thesis Committee

5-12-11
Date

ACKNOWLEDGEMENT

First and foremost, I would like to thank Jason Gurdak for the opportunity to work with him at San Francisco State University. He is truly a great teacher, mentor, and friend. I would also like to acknowledge my committee members Leonard Sklar and Peter McMahon for their timely and insightful comments that helped strengthen the manuscript. I most graciously extend my appreciation to Amber Kuss for her positive and amazing work ethic that inspired me to keep working when times were tough. Also, I would like to thank my friends and family for their everlasting support. Most of all, I would like to extend all of my gratitude to my eternal love and soul mate Emily and our sacred one, Finnegan. If not for their patience, love, and understanding this adventure would not have been possible.

TABLE OF CONTENTS

List of Tables.....	viii
List of Figures.....	ix
List of Appendices.....	xi
1. Introduction.....	1
1.1 Overview.....	1
1.2 Motivation.....	2
1.3 Mechanisms of Water Movement through the Vadose Zone.....	4
1.3.1 Uniform Flow.....	6
1.3.2 Preferential Flow.....	9
1.3.2.1 Unstable Finger Flow.....	10
1.3.2.2 Preferential Flow in Water Repellent Soils.....	11
1.3.2.3 Free-Surface Film Flow.....	12
1.3.2.4 Pore-Scale Dual-Domain Flow.....	13
1.4 Purpose and Scope.....	14
2. Site Description.....	14
2.1 Previous Studies.....	17
2.2 Techniques and Methods Used in Previous Studies.....	19
2.2.1 Chloride Method.....	19
2.2.2 Tritium Method.....	21
2.3 Conceptual Model (Arid Southwest Vadose Zone).....	22
3. Research Methods.....	23
3.1 In Situ Water Content Flux Equation.....	26
3.2 Changes in Water Content Flux Equation.....	27
3.3 Change in Storage.....	27
3.4 PET Methods.....	28

4. Results and Discussion.....	31
4.1 Deep and Rapid Wetting Fronts with In Situ Water Content	31
4.2 IMP Wetting Front Propagation with Change in Water Content.....	35
4.3 CNG Wetting Front Propagation with Change in Water Content.....	38
4.4 Changes in Water Storage Associated with Wetting Fronts.....	39
4.4.1 IMP Front #1.....	41
4.4.2 CNG Front #1.....	43
4.4.3 IMP Fronts #2–4.....	46
4.4.4 CNG Fronts #2–4.....	48
5. Supporting Evidence.....	51
5.1 Semiarid Conceptual Model.....	59
6. Conclusions.....	61
References.....	66
Tables.....	76
Figures.....	101
Appendices.....	167

LIST OF TABLES

Table 1 IMP Wetting Fronts.....	76
Table 2 CNG Wetting Fronts.....	77
Table 3–5 IMP Front #1.....	78-80
Table 6–7 CNG Front #1.....	81,82
Table 8–9 IMP Front #2.....	83,84
Table 10–11 IMP Front #3.....	85-87
Table 12–14 IMP Front #4.....	88-91
Table 15 CNG Front #2.....	92
Table 16–17 CNG Front #3.....	93-95
Table 18–19 CNG Front #4.....	96,97
Table 20–21 CNG Front #5.....	98-100

LIST OF FIGURES

Figure 1. Zero-Flux Plane Concept.....	101
Figure 2. Preferential Flow.....	102
Figure 3. Water Repellent Sandy Soil	103
Figure 4. Conceptual Model Pore-Scale Dual-Domain Flow.....	104
Figure 5. Great Plains Physiographic Province.....	105
Figure 6. Site Location Map with Precipitation Gradient	106
Figure 7. Hydrogeologic Units High Plains Aquifer.....	107
Figure 8. High Plains Aquifer Subregions.....	108
Figure 9. Characteristic Chloride Profile	109
Figure 10. Hydrostatic equilibrium model and Unit gradient model.....	110
Figure 11. HDP Preparation.....	111
Figure 12. Well Construction Diagram.....	112
Figure 13. Aluminum Housing and Concrete Pad.....	113
Figure 14. Soil Moisture Retention Curve IMP 6.4 m.....	114
Figure 15. Soil Moisture Retention Curve (RETC).....	115
Figure 16. Soil Type Distribution (IMP and CNG).....	116
Figure 17. PET Map (Dugan and Zelt, 2000).....	117
Figure 18. Mean Annual PET (Szilagyi et al. 2003).....	118
Figure 19. Location Map COMBO Method.....	119
Figure 20. IMP Total Potential Time Series	120
Figure 21. CNG Total Potential Time Series.....	121
Figure 22. Distribution of Total Monthly Precipitation.....	122
Figure 23. IMP/CNG Wetting Front Time and Depth Profiles.....	123
Figure 24. IMP Front #1 Total Potential Time Series.....	124
Figure 25. IMP Front #1 Water Flux and Change in Water Content.....	125
Figure 26. IMP Front #2 Total Potential Time Series.....	126
Figure 27. IMP Front #2 Water Flux and Change in Water Content.....	127
Figure 28. IMP Front #3 Total Potential Time Series.....	128

Figure 29. IMP Front #3 Water Flux and Change in Water Content.....	129
Figure 30. IMP Front #4 Total Potential Time Series.....	130
Figure 31. IMP Front #4 Water Flux and Change in Water Content.....	131
Figure 32. CNG Front #1 Total Potential Time Series.....	132
Figure 33. CNG Front #1 Water Flux and Change in Water Content.....	133
Figure 34. CNG Front #2,3 Total Potential Time Series.....	134
Figure 35. CNG Front #2 Change in Water Content.....	135
Figure 36. CNG Front #3 Water Flux and Change in Water Content.....	136
Figure 37. CNG Front #4 Total Potential Time Series.....	137
Figure 38. CNG Front #4 Water Flux and Change in Water Content.....	138
Figure 39. CNG Front #5 Total Potential Time Series.....	139
Figure 40. CNG Front #5 Water Flux and Change in Water Content.....	140
Figure 42-46. IMP Front #1 Change in Storage Time Steps.....	141–146
Figure 47. IMP Front #1 Available Water.....	147
Figure 48-52. CNG Front #1 Change in Storage Time Steps.....	148–152
Figure 53. CNG Front #1 Available Water.....	153
Figure 54. IMP Front #2 Available Water.....	154
Figure 55. IMP Front #3 Available Water.....	155
Figure 56. IMP Front #4 Available Water.....	156
Figure 57. CNG Front #3 Available Water.....	157
Figure 58. CNG Front #4 Available Water.....	158
Figure 59. CNG Front #5 Available Water.....	159
Figure 60. Schematic Diagram IMP Boreholes.....	160
Figure 61. GNT Total Potential Time Series.....	161
Figure 62. UMA Total Potential Time Series.....	162
Figure 63. Measured vs. Predicted Maximum Velocity.....	163
Figure 64. Wetting Front Propagation (Rimon et al., 2011).....	164
Figure 65. Chloride Profile (Rimon et al., 2011).....	165
Figure 66. Semiarid Conceptual Model.....	166

LIST OF APPENDICES

Appendix A. Soil Moisture Retention Curves.....	167
Appendix B. Annual Precipitation.....	174
Appendix C. Change in Storage Time Steps (IMP/CNG Front #1).....	181
Appendix D. Change in Storage Time Steps (IMP/CNG Fronts #2-4).....	195

1.0 Introduction

1.1 Overview

Chapter 1 will introduce the thesis and the mechanisms of water movement through the vadose zone in arid and semiarid climates. Included in Chapter 1 is the motivation for the study, which leads to the mechanisms of water movement through the vadose zone. Chapter 2 contains the site description and previous studies. Included in the previous studies are the techniques and conceptual models used estimating water fluxes through the vadose zone. Chapter 3 will outline the research methods including HDP installation, methods to estimate PET, and methods to estimate change in storage. Chapter 4 is the results and each subsequent chapter is discussion. Section 4.1 describes the total potential time series and associated water fluxes with each wetting front with an in situ estimate of water content. Section 4.2 and 4.3 describes the results of the wetting front propagation and associated water fluxes with a change in water contents. Section 4.4 describes the results of the change in storage calculation with associated wetting fronts. Chapter 5 outlines evidence that the observed spatiotemporal fluctuations in total potential indicate high water fluxes associated with the wetting front propagation down the native sediments and not due to borehole leakage. Chapter 6 outlines the conclusions of this thesis.

1.2 Motivation

To maintain the sustainability of groundwater resources in semiarid regions, it is essential to understand the interrelations among vadose zone (unsaturated zone) processes, the effects of climate on semiarid groundwater systems, and an increasing demand on groundwater resources. *Alley et al.* [1999] defines groundwater sustainability as development and use of groundwater that can be maintained for an indefinite time without causing unacceptable environmental, economic, or social consequences.

An estimated 18% of the world's population (1.1 billion of 6 billion people) did not have access to clean drinking water in 2003 [*World Health Organization—WHO*, 2003]. The *United Nations* [2004] estimated that world population could increase by approximately 47% by year 2050. Increasing water demand from a growing global population and changes to global air temperatures and precipitation patterns from climate change could have substantial effects on groundwater resources especially in semiarid regions. According to the *International Atomic Energy Agency* [IAEA, 2001], most groundwater in semiarid regions is fossil water, and use of fossil groundwater is generally unsustainable. Fossil water is groundwater that has been stored for a long period of time (10^3 – 10^6 years) [Gleick et al., 2009] and once fossil groundwater is depleted the resource will not return to previous storage in a meaningful time scale for the population using the groundwater. Therefore, accurate estimates of recharge are

imperative for sustainable management of groundwater resources in semiarid climate that are used for human consumption, irrigation, industry, and support ecosystems.

Recharge is defined as the quantity of water that crosses the boundary between the vadose zone and the saturated zone. Infiltrating water from the land surface moves downward through the underlying soil and sediments and is considered recharge when it intercepts the water table. Once the water reaches the water table it replenishes the aquifer. Therefore, it is important to quantify recharge, which is generally measured in dimensions of length per time (mm/yr). Another source of recharge is upward discharge from underlying units [*Nativ*, 1992; *McMahon et al.*, 2007] but is not relevant within the scope of this study.

Quantifying recharge is difficult and choosing an appropriate technique is important. Two factors to consider when choosing appropriate techniques include climate and the timescale of interest. First, techniques to estimate flux in arid-semiarid climates include; lysimeters, the zero-flux plane method, Darcy's law, numerical modeling, tracers (historical (^{36}Cl and ^3H) and environmental (Cl^-)) [*Scanlon et al.*, 2002], flexible time-domain reflectometry [*Rimon et al.*, 2007], hydrologic time-series approach [*Gurdak et al.*, 2007] and total potential time series. Second, temporal variability in recharge require a variety of techniques to quantify recharge depending on the timescale of interest. As outlined by *Scanlon et al.* [2002], lysimeters and zero-flux plane method are appropriate for daily to

yearly timescales. Darcy's law is appropriate for daily to century timescales. Historical tracers (^{36}Cl and ^3H) are appropriate for yearly to decadal timescales. Environmental chloride is appropriate for decadal to millennial timescales. The flexible time-domain reflectometry approach [Rimon *et al.*, 2007] and the total potential time-series approach are appropriate for daily/monthly to yearly timescales. The hydrologic time-series approach is appropriate for yearly to decadal timescales [Gurdak *et al.*, 2007]. However, climate and soil properties control the mechanisms of water movement through the vadose zone that ultimately controls the temporal variability of recharge.

1.3 Mechanisms of Water Movement through the Vadose Zone

To accurately estimate recharge rates, processes affecting infiltration and percolation through the vadose zone must be understood. The vadose zone, also called the unsaturated zone, is located between land surface and the water table and is the zone of infiltration, percolation, and recharge within an aquifer. Pore spaces in the vadose zone are unsaturated or temporarily saturated, and filled with a mixture of air, water under pressure that is less than atmospheric, and water held by capillarity [Tindall and Kunkel, 1999]. Pore spaces in sediments below the water table in the saturated zone are saturated with water under pressure that is greater than atmospheric [Tindall and Kunkel, 1999]. The

movement of water through the vadose zone to the water table is primarily controlled by pressure or potential gradients.

The zero-flux plane (ZFP) is a hypothetical horizontal plane in the vadose zone that has a total water potential (or hydraulic head) gradient equal to zero [Scanlon *et al.*, 2002], which means that fluid does not travel up or down at the ZFP. The concept of the ZFP is illustrated in figure 1 where the total water potential (hydraulic head ψ (x-axis)) is the sum of matric potential head and gravitational potential head. Matric potential results from the adsorptive and capillary forces of soil matrix properties [Tindall and Kunkel, 1999]. Gravitational potential is the potential due to the position or arbitrary reference point of soil moisture to the soil-water elevation (water table) [Tindall and Kunkel, 1999]. Above the ZFP, matric potential dominates and evapotranspiration occurs (Figure 1). Below the ZFP gravity potential dominates fluid flow and percolation can occur and recharge of the aquifer is possible (Figure 1).

The ZFP is generally located between 1 and 6 m below land surface depending on climate, soil characteristics [Wellings and Bell, 1982], and depth of root zone. However, in arid climates the location of the ZFP could be as deep as 20–40 m below land surface [Scanlon *et al.*, 1997] or not exist at all and create upward potential for water movement from the water table to the root zone [Scanlon and Goldsmith, 1997; McMahon *et al.*, 2006]. In semiarid climates, downward potential for water movement exists below the ZFP and may be

considered deep percolation [Seyfried *et al.*, 2005] and eventual recharge of the aquifer. In arid-semiarid climates the vadose zone is commonly many tens of meters thick [Scanlon *et al.*, 1997] and it may take decades to centuries [Phillips, 1994] for water to reach the saturated zone after it flows below the ZFP. It is important to note that some pore water in thick vadose zones may never reach the saturated zone under current climate conditions, and it has been suggested that recharge in some aquifers in arid-semiarid climates occurred during earlier periods of wetter and cooler climates [Smith *et al.*, 1992; Creswell *et al.*, 1999].

The rate of water movement through the vadose zone depends on uniform- and preferential-flow mechanisms. Uniform flow (also known as piston or matrix flow) in the vadose zone refers to stable, downward wetting fronts that are parallel to the land surface and often occur across the areal extent of the precipitation event [Hendrickx and Flury, 2001]. In contrast, preferential flow refers to unstable, downward wetting fronts through preferred pathways of least resistance. In general, wetting fronts travel much slower beneath uniform flow than preferential flow [Hendrickx and Flury, 2001].

1.3.1 Uniform Flow

There are many factors that affect uniform flow in vadose zones of semiarid climates including; soil texture, hydraulic conductivity, and vegetation. In general, wetting fronts propagate more deeply in coarse material. When the

soil has high levels of water content, the hydraulic conductivity is greater in coarse materials than in fine material. The larger pores in the coarse material are favorable for conducting water. However, as the material dries and the large pores empty, the hydraulic conductivity of the coarse material decreases and eventually becomes less than the fine material.

Vegetation and land use are also thought to be a major control on the location, timing, and water flux of uniform flow [Allison *et al.*, 1990; Phillips, 1994]. For example, previous studies of irrigated agricultural and rangeland settings within the northern High Plains (i.e., Nebraska) indicate the potential for downward water movement within the vadose zone, with minor seasonal variation that is consistent with quasisteady flow below the root zone [McMahon *et al.*, 2006]. Alternatively, total potential profiles beneath warmer and dryer rangeland settings of the southern High Plains (i.e., Texas) increase considerably with depth [Scanlon *et al.*, 2003; McMahon *et al.*, 2006], indicating the potential for water movement from the water table to the root zone. Scanlon and Goldsmith [1997] report similar potential profiles within interplaya settings of the southern High Plains. In general, irrigated agricultural vadose zones had larger fluxes (17–111 mm/yr) than rangeland vadose zones (0.2–70 mm/yr) [McMahon *et al.*, 2006].

Even though some previous studies have reported downward water flux and recharge beneath natural grassland settings in some semiarid regions

[*McMahon et al.*, 2006; *Scanlon et al.*, 2006; *Gurdak et al.*, 2007], the majority of studies estimate that water flux and chemical movement are greater beneath agricultural lands than beneath natural rangeland [*McMahon et al.*, 2006; *Scanlon et al.*, 2006]. However, it is important to note that many aquifers in semiarid climates have more natural rangeland than agricultural land cover. For example, across the High Plains aquifer, 56% of land is classified as rangeland, 38% as agricultural (includes irrigated and dryland), and six percent as urban and other [*McMahon et al.*, 2007]. Therefore, the overall volume of recharge may be greater under rangeland than beneath agricultural land even though average recharge rates are greater beneath irrigated land.

There are also studies that indicate that uniform flow does not contribute to recharge in arid-semiarid location around the world [*Phillips*, 1994; *Scanlon et al.*, 1999], and the transition in vegetative species at the end of the Pleistocene (~12 kyr) was a major contributor to the no-diffuse flow and recharge regimes observed at many locations [*Phillips*, 1994; *Walvoord et al.*, 2002]. Furthermore, variations in climate could have a direct effect on uniform flow. Uniform flow resulting in diffuse recharge have been observed at locations where there is ample winter precipitation and minimal evapotranspiration due to vegetation dormancy and cold temperatures, evidenced by soil water potential measurements [*Gee et al.*, 1994; *Andraski*, 1997]. Furthermore, *Small* [2005] indicates that diffuse recharge can occur at locations where precipitation is less

than potential evapotranspiration (PET) if the soil texture and climate are favorable.

1.3.2 Preferential Flow

Preferential flow is non-uniform flow that results in unstable and/or irregular wetting fronts [*Hendrickx and Flury, 2001*]. The preferential flow path may have a lower bulk density than the surrounding soil matrix resulting in a path of least resistance in which water preferentially flows [*Tindall and Kunkel, 1999*]. Thus, water movement is rapid and bypasses the bulk of the soil matrix. Understanding preferential flow mechanisms is important to accurately estimate water and solute flux through the vadose zone, recharge rates, and the quantity and quality of groundwater resources. Preferential water flow may mobilize large subsurface reservoirs of evapoconcentrated salts such as pore-water Cl^- and NO_3^- [*Hartsough et al., 2001; Walvoord et al., 2003; McMahon et al., 2006*], and/or rapidly transport land-surface derived contaminants to the water table.

Preferential flow occurs at different spatial scales (from pore to Darcian scales) (Figure 2) and is caused by different processes. Preferential flow pathways through the vadose zone include but are not limited to fractures, macropores (e.g. worm channels and root holes) [*Bouma and Dekker, 1978; Beven and Germann, 1982*] and finger flow [*Hillel, 1987*]. Furthermore, focused preferential flow occurs beneath areas where surface water collects in

topographic depressions such as ephemeral streams [Izbicki *et al.*, 2000], playas [Scanlon and Goldsmith, 1997], and depressions adjacent to leaky irrigation wells in agricultural land-use settings [Gurdak *et al.*, 2008]. The following sections describe some of the more recent and commonly reported types of preferential flow mechanisms.

1.3.2.1 Unstable Finger Flow

Previous studies suggest that the formation of fingers is due to the unstable interface between air and water that is gravity driven and is more prominent as the characteristic pore size increases [Hill and Parlange, 1972]. The fingers are considered saturated columns or “pipes” [Hill and Parlange, 1972] and the higher the flow, the wider the finger and the higher the velocity of the finger tip [Glass *et al.*, 1989a, 1989b].

Glass *et al.* [1989c] defined and outlined three stages in the evolution of the unstable flow field. The initial stage is dominated by rapid downward movement of fingers that develop finger “cores”. If supplied by a constant flow rate, the completely formed fingers preserve a constant finger tip velocity and broaden rapidly to a constant width as the finger tips propagate. Glass *et al.* [1989c] suggests that hysteresis permits the infiltrating finger to propagate with minimal lateral dispersion. The second stage is defined by the persistence of finger core regions that maintain a confluence of flow and by the onset of slow

lateral dispersion of wetting fronts which create a less saturated “fringe” region between the more saturated finger core regions. For the finger to persist it must be supplied by lateral flow of water from the fringe region in concert with the region above [Jury *et al.*, 2003]. The initial stage of downward finger formation may take minutes to develop whereas the second stage of fringe formation may take days to develop. The third and final stage is a steady-state flow regime where the core and fringe regions persist for extended periods of infiltration.

It has been documented that fingers from one infiltration occurrence remains and develops in the same location during subsequent infiltration cycle [Glass and Steenhuis, 1984; Glass *et al.*, 1987] with the core and fringe regions being preserved. The bulk of the infiltration convergence remains in the “core” region and the “fringe” region becomes more of a contributor than in the previous cycle [Glass *et al.*, 1989c].

1.3.2.2 Preferential Flow in Water Repellent Soils

In water repellent soils (Figure 3), preferential flow paths are expected to develop with the first large precipitation events after a prolonged dry period [Dekker and Jungerius, 1990]. Results of model simulations [Ritsema *et al.*, 1998] indicate that finger formation results from hysteresis in the water retention function and that the fingers recur along the same pathways during wetting and drying cycles. The wetting of the preferential pathway leaches hydrophobic

substances (humic and fulvic acid) and changes the water retention function resulting in a pathway that is more wettable than the surrounding porous media [Ritsema *et al.*, 1998].

For preferential fingers to persist after percolation subsides, the preferential pathway and the surrounding matrix dry with the end result of two zones with separate water contents and hydraulic conductivities ($K(\theta)$) [Glass *et al.*, 1989c]. The preferential pathway has a higher water content and therefore a greater $K(\theta)$ which allows a subsequent precipitation event to flow preferentially via the old pathway ("core") and the flux is equal to $K(\theta)$ in the "core" area [Glass *et al.*, 1989c].

1.3.2.3 Free-Surface Film Flow

Previous studies suggest that preferential flow through the vadose zone may not allow the transporting water sufficient time to equilibrate with the interstitial pore-water [Skopp, 1981; Jarvis, 1998]. Nimmo [2010] developed a one-dimensional source-responsive flux model based on the concept of free-surface thin film flow that is considered laminar flow that bypasses interstitial pore-water. Nimmo [2010] assumes that the media has little effect on film flow as long as it supports unsaturated flow, traditional state variables of unsaturated flow are negligible, and the flow system relies heavily on intermittent behavior of water input. Also, the concept of thin-film flow is generally referring to free-

surface films along the walls of macropores within the upper 1–3 m of a profile [Nimmo, 2010].

1.3.2.4 Pore-Scale Dual-Domain Flow

Pore-scale dual-domain flow occurs when a wetting front propagates preferentially through a thin film or “flow net” of interconnected pore spaces within the soil matrix (Figure 4) [Rimon *et al.*, 2011]. This type of flow can be observed and measured using water-content sensors (e.g., time-domain reflectometry probes (TDR) [Robinson *et al.*, 2003]) and matric-potential sensors (e.g., heat-dissipation probes (HDPs) [Gurdak *et al.*, 2007]). Using direct observations, Rimon *et al.* [2011] developed a conceptual model for pore-scale dual-domain flow. The conceptual model includes the following assumptions 1) the vadose zone never reaches complete saturation; 2) water flows primarily through a net of hydraulically interconnected pores, and these nets could persist as subsequent percolation events occur much like finger flow recurrence [Glass and Steenhuis, 1984; Glass *et al.*, 1987; Wang *et al.*, 2003]; 3) the flow nets within the pores rely on hydraulic conditions that leave portions of the pores detached from the flow net; 4) and the active flow net expands and contracts during percolation and drainage is flushed while the detached pores remain unwashed that results in the long-term accumulation of solutes. Therefore, the flow net and the soil matrix may never reach equilibrium.

1.4 Purpose and Scope

The overarching purpose of this study is to identify hydrogeologic processes and mechanisms of water movement through the vadose zone beneath two semiarid natural grassland locations—Imperial, NE (IMP) and Cimarron National Grassland, KS (CNG)—of the High Plains aquifer. I will evaluate total potential time series beneath IMP and CNG to characterize the propagation of wetting fronts and the associated response to seasonal and episodic precipitation events.

2.0 Site Description

The High Plains aquifer is located in the Great Plains physiographic province of the United States (Figure 5). Locally known as the Ogallala aquifer, this regionally important aquifer underlies approximately 450,000 km² in parts of eight states, including Colorado, Kansas, Nebraska, New Mexico, Oklahoma, South Dakota, Texas, and Wyoming. *Gutentag et al.* [1984] described the High Plains as an arid-semiarid region with plenty of sunshine, common windy conditions, moderate precipitation, low humidity, and a high rate of evaporation. Due to the large amount of area covered by the High Plains, there is a relatively steep gradient between cooler temperatures in the north and warmer temperatures in the south. Daily air temperature ranges from 15°C to 30°C and there is a relatively large (~70°C) seasonal difference between winter lows and

summer highs [Gutentag *et al.*, 1984]. The mean annual precipitation increases from west to east by roughly 2.5 cm every 40 km [Gutentag *et al.*, 1984] (Figure 6).

The High Plains aquifer comprises six hydraulically connected hydrogeologic units that mostly consist of sedimentary deposits (Figure 7) [Gutentag *et al.*, 1984]. The Ogallala Formation makes up the majority (75%) of the total area of the aquifer and consists primarily of unconsolidated clay, silt, sand, and gravel with scattered cemented zones consisting of calcium carbonate [Gutentag *et al.*, 1984].

The aquifer is a source of irrigation water for one of the most productive agricultural regions in the United States. In 2000, roughly 30% of the groundwater used for irrigation in the U.S. was pumped from the High Plains aquifer [Maupin and Barber, 2005].

I studied two natural grassland sites (IMP and CNG sites) within the High Plains (Figure 7). Previous studies in the High Plains indicate that recharge rates are greater beneath irrigated agricultural land than natural grassland sites [McMahon *et al.*, 2006; Scanlon *et al.*, 2005]. However, natural grassland is the dominant land use, accounting for approximately 56% of the land overlying the High Plains aquifer (National Land Cover Database, 2001). Of the 38% that is agricultural land, about 30% is beneath irrigated agricultural land and 8% is beneath non-irrigated (dryland) agriculture as of 1992 [Qi *et al.*, 2002]. Thus, it is

important to evaluate and understand hydrogeologic processes that occur beneath natural grasslands because they potentially account for the largest contributing area for groundwater recharge to the High Plains aquifer. Estimating water flux and recharge rates beneath natural grasslands and irrigated cropland is useful to evaluate the natural and human impact on water quality and sustainability of this important freshwater resource.

The study area for the High Plains aquifer is divided into three geographic subregions; northern High Plains (NHP), central High Plains (CHP), and southern High Plains (SHP) [McMahon *et al.*, 2007] (Figure 8). The subregions were chosen based on the regional temperature gradient. The IMP site is located in the northern High Plains, approximately 13.3 km (8.26 mi) northeast of Imperial, Nebraska (Figure 8). The CNG site is located in the Cimarron National Grasslands, within the central High Plains approximately 16.3 km (10.13 mi) northeast of Elkhart Kansas (Figure 8). The vadose zones of the two sites have very similar sandy loam soils, including sand, clay, silt, and gravel with scattered cemented zones containing calcium carbonate. The slopes of the land are flat to gently rolling and the sediments are adequately coarse for modest to high rates of infiltration. In 2000, at the time of installation at CNG the depth to water (dtw) below land surface was ~50 m [McMahon *et al.*, 2003]. In 2002, at the time of installation at IMP the dtw below land surface was ~25–28 m [McMahon *et al.*, 2006].

2.1 Previous Studies

The Regional Aquifer-System Analysis (RASA) program of the United States Geological Survey (USGS) began in 1978 [Gutentag *et al.*, 1984]. Gutentag *et al.* [1984] conducted a study on the High Plains aquifer to provide groundwater-resource managers with (1) hydrologic information needed to evaluate the effects of continued groundwater development and (2) computer models to predict aquifer response to changes in ground-water development.

More recently, the High Plains aquifer has been part of an ongoing study by the USGS on the quality of the nation's water resources. In 1991, the USGS implemented the National Water Quality Assessment (NAWQA) Program, which was designed to inform water-quality managers and policy makers about the state of the nation's water on national, regional, and local levels [McMahon *et al.*, 2007].

As part of the USGS NAWQA study of the High Plains aquifer, McMahon *et al.* [2003] compared infiltration and recharge of a natural rangeland site (CNG) to two irrigated sites within the central High Plains (CHP) aquifer study area to better understand the effects of land use on hydrogeologic processes. Methods used by McMahon *et al.* [2003] include tritium profiles, chloride profiles, total water potential, nitrate, and pesticide profiles to determine water flux rates through the vadose zone. Using the chloride mass balance (CMB) approach, McMahon *et al.* [2003] estimated the flux at CNG to be 5.1 mm/yr. In

comparison, water flux estimates at the irrigated cropland sites in the central High Plains region were 53 mm/yr and 54 mm/yr using downward displacement of chloride and tritium data, respectively. These findings by *McMahon et al.* [2003] indicate that water fluxes are substantially (1-order of magnitude) greater beneath irrigated cropland than beneath natural rangeland of the CHP.

Also part of the High Plains NAWQA program, *McMahon et al.* [2006] conducted studies on recharge rates, chemical transport and storage in the vadose zone of the High Plains aquifer. The estimated water flux using tritium data at IMP was 70 mm/yr [*McMahon et al.*, 2006]. In contrast, the estimated flux at an irrigated cropland site near Grant, NE (GNT) in the northern High Plains (NHP) was 102 mm/yr. Although not as great a difference as in the CNG, water flux estimates are less beneath rangeland sites as compared to beneath irrigated agricultural sites in the NHP. *McMahon et al.* [2006] suggests that hydrologic, chemical, and isotopic data provides evidence that preferential flow or “fast pathways” as well as “slow paths” for water movement takes place through the vadose zone of the High Plains aquifer and advective chemical transit times are between 49 and 10,500 years.

Using heat-dissipation probe (HDP) data *Gurdak et al.* [2007] reported relatively sharp- and uniform- wetting fronts in the NHP that reached depths of 6.4 to 23.0 m at an estimated water flux (from hydrologic time-series approach) ranging from 455 to 476 mm/yr. *Gurdak et al.* [2007] suggested the propagation

of the wetting fronts indicate predominantly pistonlike or matrix flow and the depths of the wetting front were greater under irrigated agricultural sites than the corresponding rangeland sites. These findings support previous findings by *Scanlon et al.* [2005] that land use is a major control on water movement in the vadose zone of the High Plains aquifer.

2.2 Techniques and Methods Used in Previous Studies

The methods used by *McMahon et al.* [2003, 2006] are tracer-based techniques for estimating water flux and recharge rates. The chloride mass balance (CMB) approach is best used in regions where there are relatively small water fluxes [*Scanlon et al.*, 2002]. The water fluxes reported using the CMB approach are estimates over decadal to millennial timescales. The tritium approach estimates water fluxes for yearly to decadal timescales [*Scanlon et al.*, 2002].

2.2.1 Chloride Method

At semiarid locations, the CMB approach can be used to determine the past water flux over millennial timescales [*Scanlon et al.*, 1997], including up to ~10-15 thousand years in some cases [*Phillips et al.*, 2004]. The major assumption of the CMB approach is that the transport process is downward

piston flow and chloride transport through the vadose zone is shown in the following equation [Scanlon *et al.*, 1997]

$$q_{cl} = q_l c_{cl} - D_h \frac{\partial c_{Cl}}{\partial z} \quad (1)$$

where q_l is the volumetric liquid water flux below the root zone ($L T^{-1}$), q_{cl} is the chloride deposition flux at the surface ($M L^{-2} T^{-1}$), c_{Cl} is the pore water chloride concentration ($M L^{-3}$), and D_h is the hydrodynamic dispersion coefficient ($L^2 T^{-1}$), which is a function of θ (volumetric water content ($L^3 L^{-3}$)) and v (average pore water velocity ($L T^{-1}$)). The hydrodynamic dispersion coefficient D_h is a composition of the mechanical dispersion coefficient D_m and the effective molecular diffusion coefficient D_e . However, due to small water flux in arid-semiarid climates, the mechanical dispersion likely has a negligible effect on the hydrodynamic dispersion coefficient [Allison and Hughes, 1978]. Therefore, equation (1) can be rearranged to

$$q_l = \frac{q_{cl}}{c_{Cl}} \quad (2)$$

Chloride deposition from precipitation, dry fallout, or irrigation will increase from the land surface down and may concentrate at the root zone due to evapotranspiration [Gardner, 1967] (Figure 9). The CMB age of the chloride spike in the profile can be determined using a combination of chloride concentrations in the shallow vadose zone with a constant atmospheric chloride input [Walvoord and Scanlon, 2004]. However, there is uncertainty in estimated

water fluxes using the CMB approach [Scanlon, 2000]. These uncertainties include Cl^- input into the system, in transport processes, and in Cl^- output or Cl^- concentrations measured in the pore water.

2.2.2 Tritium Method

Tritium (^3H) is a radioactive isotope of hydrogen. Atmospheric nuclear testing in the 1950's and 1960's produced elevated levels of tritium in precipitation (>8 TU in the High Plains region) [Thatcher, 1962], which is evident in pore water of thick vadose zones with relatively slow recharge rates [Scanlon *et al.*, 1997]. Due to the short half-life of 12.43 years, the amount of tritium in the soil will decrease because of radioactive decay. However, the low water fluxes in the vadose zones of arid and semiarid regions often result in a bulge, spike, or elevated concentrations of tritium in pore water in the upper profile near the ZFP. The elevated tritium concentrations often reflect peak atmospheric thermonuclear testing from 1963 [McMahon *et al.*, 2003].

Two methods can be used to determine water flux from tritium. When a distinct interface between postbomb and prebomb tritium is present or when a 1963 bulge is present in the profile, the water flux can be calculated with

$$q = \theta z / t \quad (3)$$

where θ is water content ($\text{L}^3 \text{L}^{-3}$), z is the depth of the interface or postbomb peak below land surface (L), and t is the elapsed time since 1953 or 1963 (T).

Equation 3 assumes that flow is one-dimensional and vertically downward, that volumetric water content is at steady state, and that vapor transport of tritium is insignificant.

2.3 Conceptual Model (Arid Southwest Vadose Zone)

The conventional hydrostatic equilibrium model and the unit gradient model (Figure 10) are two conceptual models that are frequently used to explain vadose zone total potential profiles in the arid southwestern U.S. [Walvoord, *et al.*, 2002]. The hydrostatic equilibrium model indicates no-flow conditions result when matric potential equals gravimetric potential. If this model is sufficient then matric potential profiles would plot along the hydrostatic equilibrium line due to small water flux in arid regions [Walvoord *et al.*, 2002].

The proposed unit gradient model indicates that matric potential below the root zone adds little to the total hydraulic gradient. Once past the root zone the water flux equals the unsaturated hydraulic conductivity [Gardner, 1967; Nimmo *et al.*, 1994]. The unit gradient model estimates that in a homogeneous soil profile, the recharge rate is equal to the downward water flux below the root zone [Stephens, 1996].

Scanlon *et al.* [1997] and Walvoord *et al.* [2002] report observed profiles in arid southwestern U.S. vadose zones that diverge from the linear and uniform profiles of the hydrostatic equilibrium and unit-gradient conceptual models. The

observed matric potential profiles in desert regions have very negative potentials near the surface and increase exponentially with depth. At shallow depths the potential for water to move is up, whereas at the lower part the potential is vertically down. The plane of divergent flux can be anywhere from 10–30 m under desert floor environments in the arid southwest [Walvoord *et al.*, 2002]. Likewise, matric potential measurements reported by Scanlon *et al.* [1997] indicate upward water movement in the upper ~20–40 m of thick vadose zones of the southwestern U.S.

3.0 Research Methods

In 2000 and 2002, as part of the USGS High Plains aquifer NAWQA study, HDPs (Model 229 Water Matric Potential Sensor, Campbell Scientific, Logan, UT) were installed at two natural grassland locations (CNG and IMP) to indirectly measure matric potential of soil water at various depths within the vadose zone of the High Plains aquifer. In 2006, additional boreholes were drilled at IMP and CNG to install HDPs at shallower depths to increase the measurement points of the total profile from land surface to the water table.

The IMP and CNG sites were drilled using the casing-advance or ODEX air-hammer drilling method [McMahon *et al.*, 2003; 2006]. This drilling process involves a percussion hammer that drills with a pilot bit in conjunction with an eccentric reamer at the bottom of a steel casing. The diameter of the hole is

slightly larger than the casing. The casing is simultaneously hammered upon with the pilot bit, which advances the casing down the hole to prevent the borehole from caving in on itself. A $\frac{3}{4}$ " PVC pipe with attached heat dissipation probes (HDPs) is lowered down the open borehole. Before installation, the HDPs are saturated with deionized water, implanted in silica flour and wrapped in cheese cloth (Figure 11) to ensure hydraulic contact between the probe and the surrounding sediments. After installing the HDPs and removing the steel casing, the borehole is backfilled using a very fine silica flour to ensure good hydraulic connection to the native sediments. Dry bentonite crumble is installed between the silica flour layers to seal the annular space and prevent surface or subsurface derived borehole leakage (Figure 12). Additionally, each aluminum housing unit sits atop an approximate $1 \text{ m}^2 \times 0.2 \text{ m}$ cement pad that is designed to hold the well casing and minimize surface-derived borehole leakage (Figure 13).

The heat dissipation sensor consists of a heater and a temperature gauge within a porous ceramic matrix that equilibrates to the native sediments. The sensors are capable of measuring matric potential in the range of approximately -0.01 to -100 MPa, with a sensitivity that is proportional to the matric potential [Flint *et al.*, 2002]. The sensor is heated and the rate of heat dissipation is controlled by the water content of the porous matrix. The measured thermal conductivity of the reference matrix is a function of its water content. Heat dissipation of a porous matrix in equilibrium with the soil is measured and

correlated to matric potential of the matrix using previously determined calibration equation [Flint *et al.*, 2002].

The sensors response is susceptible to temperature, pressure, and water content [Flint *et al.*, 2002]. Each HDP for this study was calibrated following methods described by Flint *et al.* [2002] at the USGS Hydrologic Research Laboratory in Sacramento, California [McMahon *et al.*, 2006] or by D.B Stephens & Associates Laboratory in Albuquerque, New Mexico. The precision of the sensors are approximately ± 1.0 m.

Matric potential is measured every 15 minutes and has been collected continuously since installation. Matric potential values are converted to total potential by adding the gravitational potential at each HDP depth to the measured matric potential values. The change in total potential over time is used to determine the change in water content of the sediments.

Soil moisture retention curves were developed and used to estimate water content. At IMP, the sediments collected at time of installation were analyzed for volumetric water content and matric potential to develop retention curves for HDPs at depths of 6.4–23.0 m (Figure 14, Appendix A.1). The volumetric water content was measured using standard methods described by Dane and Topp [2002] [McMahon *et al.*, 2006] and the matric potential was measured with tensiometers or by the filter paper method [Deka *et al.*, 1995]. The program RETC [van Genuchten *et al.*, 1991] was used to develop moisture retention

curves for the soil at depths similar to the HDPs depths of 0.5, 1.5, 2.5, and 5.0 m (Figure 15, Appendix A.2). The RETC program was also used to develop moisture retention curves for all sediment at the depths of the HDPs (0.5 m to 9.7 m) at the CNG site (Appendix A.3). The recorded percent sand, silt, and clay from *McMahon et al.* [2006] were used for CNG and IMP (Figure 16).

3.1 In Situ Water Content Flux Equation

I modified equation (3) to estimate the water fluxes of the wetting front propagation beneath IMP and CNG

$$q = \theta \frac{z}{t} \quad (4)$$

where q is the flux (mm/d), θ is the volumetric water content ($\text{cm}^3 \text{ cm}^{-3}$) at the arrival of the wetting front, z is the distance between HDPs, and t is the traveltime from t_i to t_f (t_i is time initial, t_f is time final). The initial time (t_i) corresponds with the first observed increase in total potential at 0.5 m depth. The final time (t_f) corresponds with the earliest observed increase in total potential at the final HDP in the profile to record an increase in total potential.

3.2 Changes in Water Content Flux Equation

The previous method described in section 3.1 uses in situ water content, which could overestimate water flux. Therefore I used an additional method to estimate the water flux through the vadose zone that uses the change in water content as the wetting front propagates down the profile [Rimon et al., 2007]. Therefore, equation (4) can be rewritten as

$$q = \Delta\theta \frac{z}{t} \quad (5)$$

where q is the flux, $\Delta\theta$ is the change in water content, which is the greatest increase in water content at each HDP as the wetting front propagates down through the vadose zone, z is the depth between HDPs, and t is time elapsed between initial arrival of the wetting front at each HDP.

3.3 Changes in Storage

I measured the change in volumetric water content to calculate the change in water storage in the soil column, which is the measured area under the curve between measurement points at two different times. To calculate the change in storage I used the following equation [Rick Healy, USGS, personal communication]:

$$\Delta S = \frac{0.5}{(t_1 - t_2)} \cdot \sum_{i=0}^{L-1} \Delta z_i \cdot \{\theta_i(t_1) + \theta_{i+1}(t_1) - \theta_i(t_2) - \theta_{i+1}(t_2)\} \quad (6)$$

where ΔS is change in storage, θ is volumetric water content ($\text{cm}^3 \text{ cm}^{-3}$), t is time, and Δz is change in depth between measurement points, L is the number of measurement points, which are numbered from land surface ($i=0$) downward. The results of the change in storage estimates are used as a comparison with the amount of precipitation minus potential evapotranspiration (PET) to determine if there is enough available precipitation to account for the changes in storage. Precipitation (1931–2010) for IMP and CNG was collected from the National Climate Data Centers (NCDC) database (NOAA, 2010). Meteorological station site ID 254110 was used for IMP hydrologic time series (Appendix B.1) and meteorological station site ID 142432 was used for CNG hydrologic time series and (Appendix B.2).

3.4 PET Methods

In this study, multiple methods are used to constrain PET values that are reported in the literature for the NHP (IMP site) and CHP (CNG site) regions. First, PET values were estimated using the Hargreaves (HARG) equation [Hargreaves and Samani, 1982]:

$$ET_H = f_c \frac{0.0864 R_a}{\lambda} (T_x - T_n)^{0.5} (T_m + b) \quad (7)$$

where ET_H is the computed reference evapotranspiration (ET_0 using HARG equation) estimate (mm/day); Allen et al., [1998] describes f_c as the original

calibration factor (0.0023) of the Hargreaves equation and R_a as the extraterrestrial radiation (W m^{-2}); T_x , T_n and T_m , are daily maximum, minimum, and mean air temperature ($^{\circ}\text{C}$), respectively; T_m was computed as the average of T_x and T_n (T_x and T_n values are from NCDC); $0.0864/\lambda$ was used to transform W m^{-2} to mm/day . The solar radiation data was obtained from automated weather stations that are operated by Nebraska (station ID, a251599), and Kansas (station ID, a058799) (HPRCC, 2010). I used parameter values ($f_c = 0.0023$ and $b = 17.8$) from *Martinez-Cob and Tejero-Juste* [2004], who calibrated the Hargreaves parameters for semiarid windy locations where monthly averages of wind speed are above 2 m s^{-1} .

From year 2002–2010 for IMP and CNG, annual estimates of PET using the HARG equation range from 550–635 mm/yr and 483–650 mm/yr , respectively. However, the HARG equation tends to underestimate PET in dry regions [*Jenson et al.*, 1990; *Amatya et al.*, 1995; *Droogers and Allen*, 2002]. Thus, I compare PET estimates for IMP and CNG to *Dugan and Zelt* [2000] and PET estimates for IMP with *Szilagyi et al.*, [2003].

Dugan and Zelt [2000] used a modified Jenson-Haise energy balance method of computing PET [*Jenson et al.*, 1970; *Cady and Peckenpaugh*, 1985] with the soil water simulation program (SWASP). *Dugan and Zelt* [2000] reported annual PET estimates to increase from the northeast to the southwest. They estimated mean annual PET for southwest Nebraska, where IMP is

located, to be approximately 1,300 mm/yr (51 in/yr) (Figure 17) from 1951–1980. For CNG, they estimated mean annual PET to be 1,575 mm/yr (62 in/yr) (Figure 17).

In contrast, use of the WREVAP model by *Szilagyi et al.*, [2003] indicates an increasing PET gradient in Nebraska from northwest to southeast and estimates the long-term mean annual PET to be approximately 480 mm/yr (18.8 in/yr) in the southwest region where IMP is located (Figure 18).

The PET values estimated using the HARG equation overestimate PET compared to *Szilagyi et al.*, [2003] and underestimate PET compared to *Dugan and Zelt* [2000]. Therefore, a third comparison and calculation was made for mean monthly PET estimates for IMP and CNG. *Szilagyi and Josza* [2009] used a wet-surface (WSE) derived monthly ET estimate using 8-day composite Moderate Resolution Imaging Spectroradiometer (MODIS) daytime land surface temperature data averaged over a month. The study area in which *Szilagyi and Josza* [2009] estimated ET is in the northeast region of Nebraska (Figure 19). In northeast Nebraska, *Dugan and Zelt* [2000] estimated PET to be approximately 1,000 mm/yr (Figure 17) (approximately 20% less than the IMP region and 33% less than the CNG region.) Thus, to interpolate monthly mean estimates of ET to IMP and CNG, monthly means from *Szilagyi and Josza* [2009] were increased by 20% for IMP and 33% for CNG to estimate PET. Also, *Szilagyi and Josza* [2009] used a value of zero for the months of December through February due to

negligible ET rates during the cold winter months when plants are in a dormant state. From this point forward the method of *Szilagyi and Josza* [2009] in combination with *Dugan and Zelt* [2000] is referred to as the “COMBO” method. It is important to note that the HARG and COMBO methods to estimate PET are used to estimate available water that might account for the changes in water storage and not as a comparison of methods.

The arrival of wetting fronts at subsequently deeper HDPs beneath IMP and CNG are identified by a sharp increase and/or a gradual increase in total potential. The time step (in days) between the arrival of the wetting front at each HDP are determined due to the greatest increase in total potential at each subsequent HDP in the profile. The greatest increase in total potential corresponds to the greatest spatiotemporal increase in water content (i.e. increase in water storage). For each time step the change in storage is compared to available precipitation alone, HARG estimates, and COMBO estimates.

4.0 Results and Discussion

4.1 Deep and Rapid Wetting Fronts with In Situ Water Content

Between 2006 and 2010, total potential time series indicate at least 4 major wetting fronts occurred at IMP, reaching depths of 23 m (Figure 20), and five major wetting fronts occurred between at CNG reaching depths of 7.3 m

(Figure 21). In 2003, there was an additional wetting front beneath IMP that reached 6.4 m (Figure 20). The details of the 2003 wetting front were reported by *Gurdak et al.*, [2007]. At IMP and CNG, the initiation of the observed wetting fronts began in the year 2007 during or shortly after December 2006, which was the wettest December on record for the previous 80 years (Figure 22).

At IMP and CNG, total potential values below the root zone (~1.5 m) decrease monotonically with depth and indicate a downward potential for water movement (Figure 20, 21). An increase in total potential indicates the arrival of the propagating wetting front that is lagged in time between each HDP (Figure 20, 21). The sharp increase in total potential at subsequent depths indicates relatively uniform, matrix flow during wetting front propagation. However, the apparent, rapid water flux during propagation could be indicative of non-equilibrium preferential flow (i.e., thin-film flow [*Nimmo*, 2010]). The character of these wetting fronts is similar to those reported by *Gurdak et al.* [2007] in the High Plains and *Rimon et al.*, [2007] in the central Coastal Plain of Israel. Furthermore, *Gurdak et al.* [2007] and *Rimon et al.*, [2007] both reported relatively rapid fluxes (476 mm/yr and 3,650 mm/yr, respectively) associated with the observed wetting fronts. The error range of the water fluxes was calculated using a $\pm 20\%$ difference in water content in equation (6) because water content is estimated and likely varies in space and time during the wetting front and redistribution of water in the vadose zone.

The timeline and estimated water flux using the in situ water content for the four deep wetting fronts at IMP (Table 1, Figure 23a):

- Front #1 at IMP was initially observed at 0.5 m depth on approximately 2/22/07 and the wetting front reached 23.0 m on approximately 3/16/09 (387 day traveltime). The estimated water flux was 13.6 ± 2.7 mm/d ($5,000 \pm 1,000$ mm/yr).
- Front #2 at IMP was initially observed at 0.5 m depth on approximately 4/12/08 and the wetting front reached 9.5 m on approximately 9/3/08 (144 day traveltime). The estimated water flux was 15.8 ± 3.2 mm/d ($6,000 \pm 1,000$ mm/yr).
- Front #3 at IMP was initially observed at 0.5 m depth on approximately 10/21/08 and the wetting front reached 9.5 m depth on approximately 9/20/09 (333 day traveltime). The estimated water flux was 6.8 ± 1.4 mm/d ($2,000 \pm 500$ mm/yr).
- Front #4 at IMP was initially observed at 0.5 m depth on approximately 10/4/09 and the wetting front reached 17.0 m depth on approximately 9/13/10 (344 day traveltime). The estimated water flux was 12.6 ± 2.5 mm/d ($5,000 \pm 1,000$ mm/yr).

The estimated water fluxes for the four deep wetting fronts (2006–2010) at IMP range from 6.8 ± 1.4 to 15.8 ± 3.2 mm/d ($2,000 \pm 500$ to $6,000 \pm 1,000$ mm/yr) (Table 1) and are orders of magnitude greater than previous estimates (70

mm/yr) using tritium data [McMahon *et al.*, 2006] and the hydrologic time series approach (476 mm/yr) [Gurdak *et al.*, 2007]. The total depth (m), the days of traveltime, and the flux calculations are in Table 1 for IMP.

The timeline and estimated water content using the in situ water content for the five deep wetting fronts at CNG (Table 2, Figure 23b):

- Front #1 at CNG was initially observed at 0.5 m depth on approximately 12/20/06 and wetting front reached 5.0 m on approximately 3/6/07 (76 day traveltime). The estimated flux was 18.6 ± 3.7 mm/d ($7,000 \pm 1,000$ mm/yr).
- Front #2 at CNG was initially observed at 0.5 m on approximately 7/18/08 and the wetting front reached 1.5 m on approximately 8/23/08 (36 day traveltime). The estimated flux was 5.1 ± 1.7 mm/d ($2,000 \pm 400$ mm/yr).
- Front #3 at CNG was initially observed at 0.5 m on approximately 10/15/2008 and the wetting front reached 3.5 m on approximately 1/15/09 (91 day traveltime). The estimated flux was 7.9 ± 2.6 mm/d ($3,000 \pm 1,000$ mm/yr).
- Front #4 at CNG was initially observed at 0.5 m depth on approximately 4/7/09 and the wetting front reached 7.3 m on approximately 2/13/10 (213 day traveltime). The estimated flux was 9.2 ± 1.8 mm/d ($3,000 \pm 700$ mm/yr).
- Front #5 at CNG was initially observed at 0.5 m depth on approximately 10/27/09 and the wetting front reached 2.5 m on approximately 4/25/10

(180 day traveltime). The estimated flux was 4.0 ± 0.8 mm/d ($1,000 \pm 300$ mm/yr).

At CNG, the estimated water fluxes for the five deep wetting fronts range from 4.0 ± 0.8 to 12.6 ± 3.7 mm/d ($1,000 \pm 400$ to $5,000 \pm 1,000$ mm/yr) (Table 2) and are orders of magnitude greater than previous estimates that used the chloride mass balance approach (5.1 mm/yr) [McMahon *et al.*, 2003]. The total depth (m), the days of traveltime, and the flux calculations are in Table 2 for CNG.

4.2 IMP Wetting Front Propagation with Change in Water Content

Results of IMP wetting front propagation and water fluxes calculated using the change in water content (equation 5) are shown in Figures 24–31. In this section I provide water flux estimates in mm/d and also, compare my estimates with previous studies in mm/yr. At IMP, wetting front #1 propagated to a depth of 23.0 m (Figure 24) with an average water flux of 0.9 mm/d (300 mm/yr) (Figure 25). At 7.9 m and 9.5 m there is an estimated rapid flux of 1.8 mm/d and 2.7 mm/d, respectively (Figure 25). At a depth of approximately 8.0 m there is an increase in sand and silt (Figure 16) which lies beneath a layer of high gravel content. The clay and silt retain greater amounts of water than sand and gravel which increases the hydraulic conductivity of the sediments allowing for increased fluxes of the propagating wetting front at these depths (Figure 25).

The flux of the propagating wetting front at 23.0 m decreased to 0.2 mm/d (70 mm/yr) (Figure 25). At the time the HDPs were installed at IMP, the depth to water below land surface was approximately 25–28 m [McMahon *et al.*, 2006]. Therefore, the final estimated flux of 70 mm/yr at a depth of 23.0 m is most representative of a recharge rate for IMP, and is consistent with 70 mm/yr water flux reported by McMahon *et al.* [2006] using the tritium method.

Wetting front #2 at IMP propagated to a depth of 9.5 m (Figure 26) and had an average flux of 0.3 mm/d (100 mm/yr) (Figure 27). The most rapid water fluxes of 0.4 mm/d and 0.8 mm/d (100 mm/yr and 300 mm/yr) were recorded at depths of 7.9 m and 9.5 m, respectively (Figure 27) where there is an increase in silt (Figure 16) relative to the surrounding sediments. The results indicate that the greatest flux is associated with an increase in volumetric water content of the fine sediments. The relatively rapid fluxes (100 mm/yr and 300 mm/yr) at depths of 7.9–9.5 m are consistent with estimates of recharge under playas of the dryer and warmer southern High Plains aquifer region [Gurdak and Roe, 2010]. Fluxes under playas range from 200–600 mm/yr [Scanlon and Goldsmith, 1997], 145–257 mm/yr [Wood *et al.*, 1997]. However, these rates are an order-of-magnitude greater than reported by McMahon *et al.* [2006] (70 mm/yr) and consistent with fluxes reported by Gurdak *et al.* [2007] (476 mm/yr) for this location.

Wetting front #3 at IMP propagated to a depth of 9.5 m (Figure 28) and had an average flux of 0.1 mm/d (50 mm/yr) (Figure 29). Unlike the previous two

fronts, the most rapid flux of front #3 was at a depth of 1.5 m (Figure 29). At depths of 7.9 m and 9.5 m the estimated flux was 0.2 mm/d and 0.1 mm/d (80 mm/yr and 30 mm/yr), respectively (Figure 29). These flux rates are consistent with recharge estimates for this location from *McMahon et al.* [2006].

Wetting front #4 at IMP propagated to a depth of 17.0 m (Figure 30) and had an average flux of 0.4 mm/d (100 mm/yr) (Figure 31). Similar to wetting fronts #1 and #2, the greatest fluxes were at depths of 7.9 m and 9.5 m (Figure 31) where the lithology becomes more silt and less sand. At 9.5 m the flux was roughly 500 mm/yr which is consistent with estimates from *Gurdak et al.* [2007] (476 mm/yr) At 17.0 m the estimated flux was 100 mm/yr, which is relatively consistent with previous recharge rates estimated by *McMahon et al.* [2006] for study site IMP.

At IMP between years 2006 and 2010, four significant wetting fronts propagated to depths between 9.5 m and 23.0 m on timescales of days to months. All four wetting fronts had fluxes at depth within the profile that are consistent with previous estimates of recharge for the NHP. Three of the four fronts increased in flux at 7.9–9.5 m where there is an increase in silt and clay directly below a lens of high gravel content. The relatively higher water content of the finer grained silt and clay layer may have resulted in a higher $K(\theta)$ that enabled higher water fluxes. Two of the four wetting fronts at IMP had water flux

estimates range from 100–500 mm/yr at depths consistent with regional water levels.

4.3 CNG Wetting Front Propagation with Change in Water Content

Results of CNG wetting front propagation and water fluxes calculated using the change in water content (equation 5) are shown in Figures 32–40. At CNG, wetting front #1 propagated to a depth of 5.0 m (Figure 32) with an average flux of 6.3 mm/d (2,000 mm/yr). The velocity of the front was very rapid (5.0 m in 78 days). At 5.0 m depth the flux was 2.6 mm/d (1,000 mm/yr) (Figure 33), which is orders of magnitude greater than fluxes estimated using the CMB approach (5.1 mm/yr) [McMahon *et al.*, 2003].

Wetting front #2 propagated to a depth of 1.5 m (Figure 34) in approximately 36 days and the increase in water content almost tripled (Figure 35). The estimated flux was 6.8 mm/d (2,000mm/yr). Shortly following front #2, front #3 propagated to a depth of 3.5 m (Figure 34). Front #3 had an average flux of 1.0 mm/d (400 mm/yr) (Figure 36). These two fronts came after large precipitation events (Figure 21). The propagation of front #3 was a result of front #2 large increase in water content. Therefore, the slight increase in water content of front #3 was sufficient to propagate the wetting front to 3.5 m (Figure 34). Estimated flux rates of front's #1–3 are orders of magnitude greater than previously estimated (5.1 mm/yr) using the CMB approach [McMahon *et al.*,

2003] and are equivalent to estimates previously reported in this study using in situ water content.

Wetting front #4 propagated to a depth of 7.3 m (Figure 37) and had an average flux of 0.2 mm/d (80 mm/yr) (Figure 38). At 7.3 m depth the water flux was ~130 mm/yr, which could be considered the rate of recharge for regional locations where the water table is at that level.

Wetting front #5 propagated to a depth of 2.5 m (Figure 39) and had an average flux of 0.7 mm/d (300 mm/yr) (Figure 40). The flux increased with depth and was associated with a high level of in situ water content (Figure 40)

4.4 Changes in Water Storage Associated with Wetting Fronts

I use change in storage calculations to determine if there was sufficient available precipitation to account for the change in soil water storage following wetting front propagation. The method to estimate the change in storage likely results in an overestimate due to the interpolation between measurement points. Nevertheless, the results indicate that available precipitation is generally sufficient to account for the change in water storage.

Possible sources of error that must be taken into consideration in determining whether sufficient precipitation was available to account for the estimated change in storage include

- Error in estimates of water content values due to interpretation of the soil water retention curves
- The retention curves were developed from different sources; 1) Soil properties were analyzed in the field and the lab to create retention curves for IMP HDPs 6.4–23.0 m, 2) The curves at IMP (HDPs 0.5–5.0 m) and CNG (HDPs 0.5–9.7 m) were created empirically through the program RETC based on distribution and type of sediments
- Error in the interpolation between measurement points, which likely overestimates the change in storage calculations
- Error in the precipitation values obtained from NCDC
- Error in estimating precipitation events with corresponding deep percolation events
- Error in HDP measurement
- Error in ET estimates

As a result of multiple sources of error, I will consider any estimate of precipitation or precipitation minus ET (both methods) that is within 10% of the estimated change in storage as sufficient available precipitation to account for the estimated change in water storage.

For front #1 at IMP and CNG, I provide a detailed summary of the change in storage at each time step in comparison with available precipitation. For front's #2–4 at IMP and #2–5 at CNG, I provide a condensed summary of each

time step in comparison with available precipitation. Change in storage calculations for front #1 at IMP and CNG are in Appendix C, and calculations for front's #2–4 for IMP and CNG are in Appendix D.

4.4.1 IMP Front #1

Results of IMP Front #1 are shown in Figures 41–47. At IMP, the initial wetting front of 2007 (Front #1, Table 1) had a total increase in water storage of 0.1703 m to a depth of 23.0 m over a period of 570 days (Figure 24, Table 3). The initial onset of the deep percolation was recorded on approximately 2/22/07 at a depth of 0.5 m (Figure 24). The total potential at 0.5 m peaked in approximately 15 days (Figure 24). The estimated change in water storage in the column reached 2.5 m and increased 0.0039 m (Figure 41). From 12/06–2/07 the available precipitation of 0.0612 m and the estimates from the HARG (~0.0361 m) and COMBO (~0.0612 m) methods were all sufficient to account for the calculated change in storage (Table 4).

At time step 80 days (5/13/07) the estimated increase in water storage was 0.0186 m from 0.5 m through 6.4 m depth (Figure 42). The available precipitation alone (~0.1659 m), HARG (~0.0677 m), and COMBO (~0.0744 m) methods are all sufficient to account for the change in storage (Table 4). At time step 114 days (6/16/07) the estimated increase in water storage was 0.0267 m from 0.5 m through 6.4 m depth (Figure 43). The estimates of available

precipitation (~ 0.1659 m), HARG (~ 0.0677 m), and COMBO (~ 0.0744 m) methods are all sufficient to account for the change in storage (Table 4).

At time step 131 days (7/3/07) there is a decrease in storage from the surface to 0.5 m depth (Figure 44). Thus, there is no longer added precipitation from the surface indicating that any change in storage below 0.5 m is due to drainage. The estimated increase in storage below 0.5 m through 9.5 m was 0.0326 m (Figure 44). Estimates of available precipitation (~ 0.4279 m), HARG (~ 0.1840 m), and COMBO (~ 0.0896 m) method are all sufficient to account for the change in storage (Table 4).

A ZFP developed at 1.5 m on approximately 8/1/07 (Figure 24) and indicates an upward water potential gradient at depths less than 1.5 m. At time step 170 days (8/11/07) the estimated increase in water storage below the ZFP to 17.0 m was 0.1806 m (Figure 45). The available precipitation from 12/06–6/07 (~ 0.4270 m) and the HARG method (~ 0.1840 m) are sufficient to account for the estimated change in storage. At time step 170 days, estimated available precipitation from the COMBO method (~ 0.0896 m) is insufficient to account for the change in water storage (Table 4).

At time step 186 days (8/27/07) the estimated change in water storage between 1.5 m and 23.0 m was 0.1977 m (Figure 46). Available precipitation alone (~ 0.4270 m) and from the HARG method (~ 0.1840 m) are sufficient to account for the change in storage. Available precipitation from the COMBO

method (~ 0.0896 m) is insufficient to account for the increase in storage (Table 4).

Each subsequent time steps of 373 days, 423 days, and 570 days have a change in storage from 1.5–23.0 m depth (Table 3). Although there is an increase in relative water storage over time (373–570 days), the wetting front propagates (or drains) down the profile resulting in a decrease in water content with depth due to processes of hysteresis (Appendix C7–C9). The available precipitation alone and from the HARG method is sufficient to account for the estimated change in storage. The COMBO method of estimating available precipitation fails to account for the change in storage (Table 4 and 5).

For IMP front #1, the change in water storage at 10 of 10 time steps (100%) can be accounted for by precipitation alone and available water estimates using the HARG method (Figure 47). The COMBO method began to fail at the 5th time step at 170 days (Figure 47). Furthermore, there is an increase in total water storage at each subsequent time step due to continuing infiltration from the land surface and/or the mobilization of in situ water from the propagating wetting front.

4.4.2 CNG Front #1

Results of CNG Front #1 are shown in Figures 48–53. At CNG, the initial wetting front of 2006–2007 (Front #1, Table 2) had a total increase in water

storage of 0.1592 m to a depth of 9.7 m over 233 day traveltime (Figure 48, Table 6). However, the observed increase in total potential for front #1 indicates the wetting front only reached a depth of 5.0 m (Figure 32). Therefore, the increase in storage beyond that depth could be associated with the error in the interpolation between measurement points (Figure 48).

At time step 12 days (1/1/07) there was an increase in water storage of 0.0506 m to a depth of 2.5 m (Figure 49). After 12 day traveltime, the estimated amount of precipitation available for infiltration was 0.1737 m (Table 7). Accounting for ET using HARG (~0.1284 m) and COMBO (~0.1298 m) estimates, there was sufficient precipitation available to account for the change in storage through 2.5 m (Table 7).

At time step 24 days (1/13/07) an increase of water storage is estimated to be 0.2401 m to a depth of 2.5 m (Figure 50). After 24 day traveltime the increase in water storage of 0.2401 m is greater than the estimated available precipitation (~0.1737 m), HARG equation (~0.1284 m), and COMBO method (~0.1298 m) (Table 7).

At time step 61 days (2/19/07) the change in storage is approximately double the available precipitation (Appendix C12). After 61 day traveltime the greatest increase in total potential is at 2.5 m and the relatively large discrepancy between storage and available precipitation could be due to the mobilization of in

situ water and/or an overestimate of the change in storage due to the interpolation error between measurement points.

The top of the profile begins to dry out and a ZFP developed at 1.5 m depth on approximately 5/31/07 (Figure 32), and the potential for water movement is now up for the upper portion of the profile. Thus, only precipitation from 10/06–5/07 is available to account for the change in storage at depths below 1.5 m.

At time step 182 days (6/20/07) the estimated change in storage below 1.5 m through 7.3 m is 0.2951 (Figure 51). The available precipitation from 10/06 through 5/07 is 0.3147 m, which is sufficient to account for the change in storage. However, the HARG (~0.1519 m) and COMBO (~0.1590 m) ET estimates indicates that there is not sufficient available precipitation to account for the change in storage (Table 7).

At time step 233 days (8/20/07), the estimated change in storage below 2.5 m through 9.7 m is 0.1613 m (Figure 52). The estimated available precipitation alone is ~0.3147 m, which is sufficient to account for the change in storage. In addition, available precipitation from the HARG method (~0.1519 m) and the COMBO (~0.1590 m) method are within the estimated 10% error range (Table 7) to account for the change in storage.

For the initial wetting front of 2006–2007 at CNG, precipitation alone can account for the change in storage three out of the five time steps (60%) (Figure

52). When ET estimates were included, the HARG and COMBO method could account for the estimated increase in water storage two out of the five time steps (40%) (Figure 53). For CNG front #1 the change in storage increases with time even after a ZFP develops roughly on 5/31/07. At time step 182 days—after the ZFP develops—the change in storage continues to increase. Therefore, since no new precipitation is infiltrating beyond 1.5 m, it seems logical that in situ water that is being mobilized by the propagation of the wetting front adding to the increasing storage at depth.

4.4.3 IMP Fronts #2–4

Results from IMP Fronts #2–4 are shown in Figures 54–56. IMP front #2 had an increase in total potential observed to reach a depth of 9.5 m over a 234 day period (4/11/08–12/21/08) (Figure 26). Due to the development of the ZFP at approximately 143 days, the final time step (234 days) had an estimated increase in storage of 0.0143 m between 2.5 m and 9.5 m depth (Table 8). For front #2 there were change in storage calculations for five time steps (75, 92, 143, 212, and 234 days). Estimated available precipitation (1/08–8/08) is sufficient to account for the estimated change in storage at each time step (Figure 54) (Table 9). The HARG and COMBO methods for estimating available precipitation were sufficient to account for the increase in storage for the final three time steps (143, 212, 234 days) (Figure 54) (Table 8).

IMP front #3 had an increase in observed total potential to a depth of 9.5 m over a 451 day period (10/21/08–1/16/10) (Figure 28). There were three time steps recorded for front #3 (130, 405, and 451 days). The change in storage began to decrease at 7.9 m resulting in an increase in storage to a depth of approximately 6.4 m (Table 10). When the initial time step (130 days) was recorded the water content at 7.9–9.5 m depth was relatively high. Between time steps 130 and 451 days water had drained at depth and rewetted when the wetting front propagated to 7.9–9.5 m resulting in an increase in water content but not an increase in storage. Therefore, an overall decrease in storage was calculated at 7.9–9.5 m depth (Figure 28). A ZFP developed on approximately 9/1/09 (Figure 28) which means available precipitation for each time step is from 8/08–8/09 (Table 11). Available precipitation alone is sufficient to account for the increase in storage at each time step for front #3 (Table 11). However, neither the HARG method nor the COMBO method has sufficient available precipitation to account for the estimated increase in storage for front #3 (Figure 55) (Table 11).

IMP front #4 had an increase in total potential observed to a depth of 17.0 m over a period of 396 days (10/4/09–11/5/10) (Figure 30) and an increase in total storage of 0.1559 m to a depth of 23.0 m (Table 12). There were a total of seven time steps (156, 169, 236, 268, 308, 370, and 396 days) calculated for estimated increase in storage. The estimated available precipitation from

precipitation was sufficient to account for the estimated increase in storage at each time step for front #4 (Figure 56) (Table 13). The available precipitation from the HARG method was sufficient for five of the seven time steps. The negative value for time step 236 (5.0 m) (Figure 56) was within the 10% estimated error range (Table 12). The available precipitation from the Combo method was sufficient for three of the seven time steps (Figure 56). Time steps 308 days (7.9 m) and 396 days (17.0 m) the COMBO estimate is within the 10% error range (Table 14).

In total, estimated change in storage was calculated for 26 time steps over the four separate wetting fronts at IMP. Available precipitation alone was sufficient to account for 26 out of the 26 time steps (100%). Available precipitation from the HARG method was sufficient to account for 17 of the 26 time steps (65%). Available precipitation from the COMBO method was sufficient to account for 11 of the 26 time steps (42%). (All change in storage calculations for IMP Front's #2–4 are in Appendix D)

4.4.4 CNG Fronts #2–4

Results from CNG Fronts #2–4 are shown in Figures 57–59. CNG front #2 had the greatest increases in observed total potential to a depth of 1.5 m over a period of 51 days (7/18/08–9/7/08) (Figure 34) (Table 15). Front #3 propagated shortly after front #2 (Figure 34) over a 166 day period and the

change in water storage was very slight in comparison to front #2 (Table 16). The wetting front propagated to a depth of 3.5 m and the change in storage was observed to a depth of 7.3 m. The change in storage to a depth of 7.3 m was 0.1544 m. Estimates of available precipitation alone and from the HARG method were sufficient to account for the change in storage (Figure 57, Table 17).

CNG front #4 had observed increase in total potential at 7.3 m depth over a 393 day period (4/7/09–5/4/10) (Figure 37) resulting in an increase in storage beyond 7.3 m (Table 18). However, measurements at 0.5–2.5 m indicate that the upper section of the profile begins to dry out on approximately 5/24/09 and it is assumed that no more precipitation entered the system at depth. Therefore, available precipitation is estimated to be from 2/09 to 5/09 (Table 19).

Changes in water storage were calculated for six time steps (20, 26, 47, 140, 362, and 393 days). Results from the storage calculations indicate that precipitation alone is sufficient to account for the change in storage at each time step (Figure 58). Estimates of available precipitation from the COMBO method were sufficient for three of the six time steps (Figure 58) (Table 19). However, estimates of available precipitation from the HARG method were insufficient for all six time steps (Figure 58) (Table 19).

At CNG front #5 had observed total potential increase to a depth of 2.5 m over a period of 212 days (10/27/09–5/27/10) (Figure 39) resulting in an increase in storage beyond 2.5 m (Table 20). Change in water storage was calculated for

three time steps (158, 194, and 212 days). For the initial time step (158 days) all three methods to estimate available precipitation resulted in sufficient amounts of precipitation (Table 21) to account for the estimated increase in water storage (Figure 58). For time steps 194 and 212 days precipitation alone was sufficient to account for the estimated increase in storage (Figure 59).

At CNG, in total there were five wetting fronts that propagated to depths of 2.5 m or greater. The results from the water storage calculations reveal that available precipitation alone is sufficient to account for the change in storage at depth. Overall, water storage was calculated for 19 time steps. Fifteen of the 19 time steps (79%) had sufficient available precipitation to account for the estimated change in storage. When accounting for ET from the two methods (HARG and COMBO), the percentage of time steps that have sufficient precipitation decreases. Using the HARG method 6 of 19 time steps (32%) had available precipitation sufficient to account for the increase in storage. The COMBO method had sufficient available precipitation to account for the increase in storage for 6 of 19 time steps (33%). All change in storage calculations for CNG Fronts #2–4 are in Appendix D.

5.0 Supporting Evidence

Due to the fact that estimated water fluxes at IMP and CNG (Tables 1 and 2) are orders of magnitude greater than previously reported water fluxes at these two locations [McMahon *et al.*, 2003; 2006; Gurdak *et al.*, 2007] or elsewhere in the High Plains aquifer [Gurdak and Roe, 2010], additional evidence is needed to support the primary hypothesis that temporal changes in matric potential reflect actual water fluxes in the native sediments. The alternative hypothesis is that changes in matric potential reflect water fluxes due to borehole leakage. Although direct evidence in support of either hypothesis is impractical without destructive methods at the IMP and CNG sites, the following indirect evidence is offered in support of the primary hypothesis and simultaneous rejection of the alternative hypothesis.

Precipitation amounts were well above average during the months immediately preceding the rapid, deep wetting fronts that began in 2006 and 2007. For example, December 2006 was the wettest December on record for the previous 80 years (Figure 22a and 22b). It appears that it would not take record precipitation to cause failure of multiple boreholes at several locations at the same time and failure would have occurred sometime prior to December 2006.

At IMP, two separate boreholes drilled in 2002 and 2006 with installed HDPs are roughly 2 m apart from one another (Figure 60). The distance between the two boreholes is sufficient to ensure similar soil hydraulic properties

but an adequate amount of distance apart to ensure the installation process of the second borehole did not disturb the original borehole. Thus, the observed wetting fronts at IMP are being measured simultaneously from two boreholes roughly 2 m apart from one another.

To further explore the possibility of near simultaneous failed boreholes at IMP and CNG, I analyzed two additional sites within the vadose zone monitoring network [McMahon *et al.*, 2006] Grant, NE (GNT) and Yuma, CO (UMA)) for wetting front propagation that coincides with December 2006 record precipitation. The results indicate at GNT, which is located approximately 37 km (23 mi) north of IMP, a sharp increase in total potential occurred at depth after December 2006 (Figure 61). The total potential increase is lagged in time at subsequent depths as shown by the increase at 3.4 m, 7.6 m, 16.8 m, 22.9 m, and 29 m (Figure 61). At UMA, which is approximately 102 km (63 mi) southwest of IMP, the data indicates there is an increase in total potential at 3.4 m and 9.5 m after December 2006 (Figure 62).

Furthermore, at IMP the infiltration would've had to breach 15 layers of bentonite crumble in the original borehole that was drilled in 2002 (Figure 12) and at least 6 layers of bentonite crumble in the new borehole, which was drilled in 2006. At CNG, which is approximately 382 km (237 mi) south of IMP, at least 5–7 layers of bentonite crumble would need to fail for borehole preferential flow pathways to open. The site installations at GNT and UMA are similar to IMP and

CNG in that the HDPs are separated by multiple layers of bentonite crumble. Thus, the alternative hypothesis seems highly unlikely because borehole leakage would have had to occur through multiple layers of bentonite crumble at multiple sites separated by hundreds of kilometers, at near simultaneous times after December 2006.

Additionally, a review of the literature reveals that non-equilibrium preferential flow mechanisms and predictions of maximum transport rates could account for the observed water fluxes that are orders of magnitude greater than those estimated using tritium and CMB methods. The term preferential flow refers to unstable, non-uniform flow resulting in irregular wetting. As previously discussed, there are multiple types of preferential flow at different spatial scales (Pore, and Darcian scales) and each are caused by different processes that result in a variety of patterns.

Due to the depth of percolation recorded in this study (beyond worm channels and root holes) and the location of the study area on the stable craton of North America (lack of deep fractures), mechanisms of macropore flow is assumed to not be a major contributor at depth in locations immediately near the study sites. However, macropore flow through root holes and worm channels may be a mechanism to initiate preferential flow and may act simultaneously with other types of preferential flow leading to the observed deep and rapid percolation at CNG and IMP.

Unstable flow is frequently observed in coarse-textured media, layered media, and induced by water repellent soil and sediment [*Hendricks and Flury, 2001*]. Due to the nature of sediments at IMP and CNG, it is logical that unstable, non-equilibrium preferential flow is a possible mechanism to account for the reoccurring rapid and deep percolation observed between 2006 and 2010. It has been well documented that unstable preferential flow fingers develop and propagate in initially dry and water repellent sandy soils [*Ritsema et al., 1993; Hendricks et al., 1993; Flury et al., 1994; Ritsema and Dekker 1994; Rezanezhad et al., 2006*] similar to the lithology at IMP and CNG (Figure 3). The increase in water content increases the unsaturated hydraulic conductivity resulting in fairly rapid fluxes through the finger. Previous studies report a flux rate of approximately 1,472 mm/yr in the initial ~1 m of fine sand in the Netherlands [*Ritsema et al., 1993*], which is relatively consistent with water flux estimates from IMP and CNG.

Previous studies suggest that rapid water fluxes through the vadose zone do not allow the transporting water sufficient time to equilibrate with the water in the adjacent matrix material [*Skopp, 1981; Jarvis, 1998*]. This is consistent with the rapid fluxes recorded in this study ($1,000 \pm 400$ mm/yr to $6,000 \pm 1,000$ mm/yr) which is not recorded using tracer-based techniques (5–70 mm/yr) [*McMahon et al., 2003, 2006*]. The non-equilibrium preferential flow could bypass the pore-water containing the tritium or chloride leaving the solute behind which would

account for the slower rates reported using the CMB and tritium approach for estimating flux and adding to the uncertainty of estimating water fluxes using environmental tracers [Scanlon, 2000]. Furthermore, as suggested by Wood [1999], reported fluxes from Scanlon and Goldsmith [1997] using the CMB approach are matrix flux estimates (60–100 mm/yr). Within 10 km of Scanlon and Goldsmith [1997] study sites, Wood [1997] used physical, chemical, and isotopic methods to estimate fluxes that range from 750–2,720 mm/yr. Wood [1997] concluded that if the flux and recharge beneath playa floors are estimated from only the CMB approach or the tritium method, the results are significantly underestimated due to the occurrence of macropore flow. Thus, it is also important to note that tracer-based techniques record water fluxes over decadal to millennial timescales, which represents periods of rapid water flux as well periods with little to no water flux.

In addition to providing supporting evidence that the rapid fluxes aren't a product of borehole leakage, I estimated and predicted the maximum velocity of water for each observed wetting front at IMP and CNG using an equation from Nimmo [2007]. The equation is tailored toward systems where water input is intermittent. Assumptions are made that input occurs in hypothetical pulses during which the tracer's speed is constant and between which it is negligible. Therefore, the empirically estimated universal constant of 18 was used for the ratio V_O/i_O in equation [Nimmo, 2007]

$$V_{\max-pred} = V_o \frac{i_{avg}}{i_o} \quad (7)$$

where i_{avg} is the actual average input rate, I_{total}/t_f . I_{total} is the amount of water input during the transport process from time 0 to time final (t_f).

Results indicate 9 of 9 measured velocities from IMP and CNG are within one order-of-magnitude of the predicted velocities using equation (7) (Figure 63). Furthermore, the predicted and measured velocities from IMP and CNG are comparable to data from *Jury et al.* [1982] from Etiwanda, CA, which has similar lithology and climate to IMP and CNG. *Jury et al.* [1982] reported an estimated maximum velocity of 0.05 m/d with 210 mm of rain and 0.04 m/d with 150 mm of rain. The minimum measured velocity from IMP and CNG was 0.01 m/d with approximately 170 mm of precipitation and the maximum measured velocity from IMP and CNG was 0.06 m/d with approximately 90 mm of precipitation (Figure 63). *Nimmo* [2010] suggested that source-responsive thin-film flow could account for these rapid velocities.

The concept of thin-film water movement through moderately wet porous media at depth seems realistic when the smaller pores are completely filled with water and a thin film flows over the surface of the larger pores [*Lebeau and Konrad*, 2010]. Furthermore, in moderately dry to dry media, thin-film flow may continue along dry particles by adsorptive forces that are greater than capillary forces during the nonwetting phase [*Lebeau and Konrad*, 2010].

The results of this study are consistent with the proposal that thin-film flow rapidly bypasses or incompletely flushes the soil matrix leaving behind most of the solutes that have accumulated in the pore water. Some dissolved ions such as chloride and nitrate in pore-water chemistry may equilibrate with the thin-film flow and be mobilized downward, causing a vertical spreading of the pore-water chemistry profiles in the vadose zone that is consistent with hydrodynamic dispersion. In general, pore-water chloride and tritium profiles have elevated concentration near the ZFP and a gradual decline in solute concentration below the peak concentration (Figure 9). The chloride concentrations in the profile beneath the peak concentration are likely the result of bypassing thin-film flow that mobilizes a small fraction of the solute further down the profile. However, the majority of the dissolved ions in the pore water does not reach equilibrium with the rapidly flowing thin-film flow and remains immobile within pore-water that is tightly held in the smallest pores of the vadose zone sediments. Thus, techniques that use environmental tracers (such as chloride or tritium) to estimate flux rates through the vadose zone may not necessarily account for thin-film flow that bypasses or incompletely flushes the interstitial pore water and may result in an underestimation of water flux [Wood, 1999].

Moreover, the previous interpretation of vadose zone processes has been validated by the pore-scale dual-domain flow conceptual model developed by *Rimon et al.* [2011]. In Israel, at a semiarid location with similar lithology as the

High Plains aquifer, *Rimon et al.* [2007] observed very similar propagation of wetting fronts to approximately 21 m (Figure 64) with a water flux estimate of 10.2 mm/d (3,723 mm/yr).

The development of *Rimon et al.* [2007] vadose zone monitoring system included vadose-zone sampling ports (VSPs) [*Rimon et al.*, 2011] that allowed sampling of vadose-zone pore water on a regular basis [*Dahan et al.*, 2009]. The sampling of the pore water allowed *Rimon et al.* [2011] to characterize the chemical composition of the percolating water through the vadose zone. The results indicate a large discrepancy between chloride concentrations of the sediment samples collected during borehole drilling and the pore water sampled from the VSPs. Throughout the entire 21 m profile the chloride concentration was greater from the sediment samples than from the pore water sampled from the VSPs. Furthermore, chloride concentrations in the groundwater were also less than the chloride concentrations in the sediment samples (Figure 65). Those results are consistent with reports from the USGS vadose zone network. [*McMahon et al.* 2007]. *McMahon et al.*, [2006 reported a discrepancy between high concentration of agricultural in young groundwater (<50 yrs) and estimated advective chemical transport (49-10,500 yrs) through the vadose zone of the High Plains aquifer [*McMahon et al.*, 2006].

In this study I interpreted the processes responsible for rapid water flux and apparent discrepancies between observed groundwater chemistry and

chemical fluxes through the vadose zone of the High Plains aquifer as thin-film flow [Lebeau and Konrad, 2010; Nimmo, 2010] at the pore scale. I suggest that the thin-film flow bypassed the pore-water containing concentrations of chloride and tritium that are measured to estimate water flux from conventional tracer-based techniques. *Rimon et al.* [2011] described the same type of process as pore-scale dual-domain flow and developed a conceptual model with certain assumptions, which were described in section 1.3.2.4 in this paper. All of which are included in my new semiarid conceptual model for water movement through the vadose zone.

5.1 Semiarid Conceptual Model

In general, previous studies conducted in semiarid regions generally follow the conceptual model of arid regions, such as the southwestern U.S. However, *McMahon et al.* [2006] proposed a conceptual model that defines slow and fast “pathways” of downward water movement through the vadose zone of the High Plains aquifer. The fast pathways were believed to be primarily beneath irrigated cropland (timescales of possibly months to decades) and focused flow beneath depressions, ephemeral streams, and playas (timescales of years to centuries).

To my knowledge, no prior studies have directly proposed or defined a conceptual model of semiarid regions that suggest rapid wetting front propagation can occur in the soil matrix without defined “pathways” through the

vadose zone. However, *Rimon et al.* [2011] proposed a conceptual flow and transport model based on observed wetting front propagation that was controlled by matrix flow as well as chemical characteristics that indicate preferential flow. *Rimon et al.* [2011] identified this process as “pore-scale dual domain flow” through the vadose zone. Similarly, I observed relatively sharp increases in total potential that indicate the propagation of the multiple uniform wetting fronts and matrix type flow. However, the rapid water flux estimates indicate that preferential flow was the mechanism of water movement.

Furthermore, the results of the total potential times series from this study indicate that the potential for water movement is down beneath two semiarid climate locations above the High Plains aquifer. The downward potential and the observed multiple deep wetting fronts do not support the use of the arid southwestern conceptual model. Thus, I propose to define a new conceptual model for water movement through the vadose zone of the semiarid region of the High Plains aquifer.

The primary focus of the new semiarid conceptual model explores the occurrence and mechanisms of rapid and deep wetting fronts within the vadose zone of the High Plains aquifer. The new semiarid conceptual model for water movement is based on decreasing total potential with depth. The decrease in total potential indicates the potential for water movement is down and that recharge is possible under current climate conditions. Also, the mechanisms of

water movement could be threefold 1) uniform, matrix type flow 2) preferential flow and 3) pore-scale dual-domain flow. These three types of flow are likely to be working in sync with one another throughout the vadose zone from land surface to the water table. However, the results from this study indicate that pore-scale dual-domain flow is likely the main contributor to deep and rapid wetting front propagation and follow the assumptions made by *Rimon et al.* [2011] (Figure 66).

6.0 Conclusions

The overarching goal of this study was to characterize the hydrogeologic processes and mechanisms of water movement through the vadose zone of the High Plains aquifer. The total potential time series indicated the recurrence of previously unobserved deep percolation events which warranted a collection of evidence to support the hypothesis that water movement was through the native sediments and not due to borehole leakage. Also, the evaluation of mechanisms of water movement have helped explain the hydrogeologic processes responsible for the previously unobserved deep and rapid wetting fronts at study sites IMP and CNG of the High Plains aquifer. As a result, the objective of the study was to develop and validate a new semiarid conceptual model for water movement through the vadose zone of semiarid regions.

The use of HDPs to measure matric potential (converted to total potential) of the vadose zone at two natural rangeland sites within the regionally important High Plains aquifer have been important to identify the recurrence of previously unobserved rapid and deep percolation and propagation of wetting fronts. The results indicate that water movement is orders of magnitude greater than previously estimated using tracer-based techniques to estimate water flux. The initial onset of these reoccurring wetting fronts came during or directly after December 2006, which was the wettest on record for the previous 80 years.

Initially, the water flux was estimated using the in situ volumetric water content of when the wetting front arrived at each HDP. By using the in situ water content at the time of arrival grossly overestimated the water fluxes by a predicted order-of-magnitude. Therefore, an alternative technique was used to determine the water flux at each HDP in the profile. An alternative value of water content was determined by the maximum change in water content as the wetting front propagated down the profile. This new value of water content is a more realistic representation of the volume of water contained in the propagating wetting front.

At IMP the increase in water content was not as great as what was recorded from site location CNG. The fluxes at IMP were at times consistent with previous estimates using the tritium approach [McMahon *et al.*, 2006] and hydrologic time series approach [Gurdak *et al.*, 2007] but also were orders of

magnitude greater ($\sim 1,000$ mm/yr). However, the consistency between these results (450 mm/yr) and *Gurdak et al.* [2007] (476 mm/yr) further demonstrate some limitations of tracer-based techniques for estimating water flux through the vadose zone of the High Plains aquifer on daily to annual timescales. Furthermore, the results at IMP are consistent with thin-film flow that bypasses the soil matrix and is a viable mechanism responsible for the observed recurring deep percolation and rapid wetting fronts that are undetected by conventional tracer-based techniques for estimating water flux.

At times beneath CNG, water content increased three-fold and resulted in water fluxes that are orders of magnitude greater than previously reported. CNG was initially relatively dry and the significant increase in water content resulted in rapid water flux estimates. Again, these recurring deep and rapid fluxes support the proposal that thin-film flow is rapidly bypassing the soil matrix leaving behind solutes that are measured when using tracer-based techniques for estimating water fluxes through the vadose zone.

By and large, the results of this study provide sufficient evidence that support a new conceptual model of water movement through the vadose zone of semiarid regions. Most notably, there is a strong and consistent potential for downward movement of water to the water table. A significant precipitation event is capable of increasing the water content and therefore unsaturated hydraulic conductivity of the sediments to levels that support the reoccurrence of rapid and

deep percolation. Lastly, the propagation of the wetting fronts could be moving along thin films at the pore scale—also known as pore-scale dual-domain flow—that rapidly bypass the interstitial pore water leaving behind solutes.

The movement of water on daily to annual timescales has implications for the enhanced mobilization of some fraction of contaminants in the vadose zone to groundwater resources, and should be considered by water managers and policy makers. Most notably, interpretations of the observations and reported water fluxes from this study may account for the marked inconsistency between observed groundwater chemistry and previously estimated chemical fluxes in the vadose zone of the High Plains aquifer [Gurdak *et al.*, 2008]. Elevated concentrations of nitrate and pesticides have been measured in recently recharged groundwater (<50 yr in age based on tritium) of the High Plains aquifer [McMahon *et al.*, 2007]. Measured concentrations of these agrichemicals in groundwater are not consistent with the previous estimates of advective chemical transit times ranging from 49 to 10,500 yr [McMahon *et al.*, 2006; Gurdak *et al.*, 2007]. The advective chemical transit times were estimated from measured tritium and chloride profiles in the relatively thick (15–60 m) vadose zones beneath a number of natural rangeland and irrigated agriculture settings [McMahon *et al.*, 2006; Gurdak *et al.*, 2007]. The calculated advective chemical transit times are commonly greater than the time since the onset of extensive irrigated agriculture on the High Plains approximately 50 to 60 yr ago. However,

estimated water fluxes from this study indicate much more rapid transit times that could account for the presence of the measured concentrations of agrichemical in groundwater of the High Plains aquifer.

Extended continuous monitoring of total potential is needed to evaluate the temporal variability of the observed deep and rapid wetting front propagation. Furthermore, comparing the results of the total potential time series with chloride and tritium at IMP and CNG could provide further valuable information on all possible mechanisms controlling the movement of water. It would be interesting to observe whether the reoccurring deep wetting is flushing the pore-water or simply bypassing the soil matrix as predicted in this study. Extending this type of study to other semiarid regions may be useful in evaluating water movement through the vadose zone, recharge beneath natural environments, and ultimately estimate a portion of the global groundwater budget.

References

- Allen, R. G., L. S. Pereira, D. Raes, M. Smith, and others (1998), Crop evapotranspiration-Guidelines for computing crop water requirements-FAO Irrigation and drainage paper 56, *FAO, Rome*, 300.
- Alley, W. M., T. E. Reilly, and O. L. Franke (1999), Sustainability of ground-water resources, US Dept. of the Interior, US Geological Survey Circular 1186, 79 p.
- Allison, G.B., and M.W. Hughes (1978), The use of environmental chloride and tritium to estimate total recharge to an unconfined aquifer, *Australian Journal of Soil Research*, 16(2), 181-195, doi10.1071/SR9780181.
- Allison, G. B., P. G. Cook, S. R. Barnett, G. R. Walker, I. D. Jolly, and M. W. Hughes (1990), Land clearance and river salinisation in the western Murray Basin, Australia, *Journal of Hydrology*, 119(1-4), 1-20.
- Amatya, D. M., R. W. Skaggs, and J. D. Gregory (1995), Comparison of methods for estimating REF-ET, *Journal of irrigation and drainage engineering*, 121(6), 427-435.
- Andraski, B. J. (1997), Soil-water movement under natural-site and waste-site conditions: A multiple-year field study in the Mojave Desert, Nevada, *Water Resour. Res.*, 33(8), PP. 1901-1916,doi:199710.1029/97WR01502.
- Beven, K., and P. Germann (1982), Macropores and water flow in soils., *Water Resources Research*, 18(5), 1311-1325.
- Bouma, J., and L. W. Dekker (1978), A case study on infiltration into dry clay soil I. Morphological observations, *Geoderma*, 20(1), 27-40.
- Cresswell, R., J. Wischusen, G. Jacobson, and K. Fifield (1999), Assessment of recharge to groundwater systems in the arid southwestern part of Northern Territory, Australia, using chlorine-36, *Hydrogeology Journal*, 7(4), 393-404.

- Cady, R. E., and J. M. Peckenpaugh (1985), Documentation of RAQSIM—A Regional Aquifer Simulation Model and Its Use in the Twin Platte-Middle Republican Study Area, Nebraska, *US Geological Survey Water-Resources Investigations Report*, 85, 4168.
- Dahan, O., R. Talby, Y. Yechieli, E. Adar, N. Lazarovitch, and Y. Enzel (2009), In situ monitoring of water percolation and solute transport using a vadose zone monitoring system, *Vadose Zone Journal*, 8(4), 916.
- Dane, J. H., G. C. Topp, G. S. Campbell, R. Horton, W. A. Jury, D. R. Nielsen, H. M. van Es, P. J. Wierenga, and G. C. Topp (2002), Part 4: Physical methods, *Methods of Soil Analysis*.
- Deka, R. N., M. Wairiu, P. W. Mtakwa, C. E. Mullins, E. M. Veenendaal, and J. Townend (1995), Use and accuracy of the filter-paper technique for measurement of soil matric potential, *European Journal of Soil Science*, 46(2), 233–238.
- Dekker, L. W., and P. D. Jungerius (1990), Water repellency in the dunes with special reference to The Netherlands., *Catena, Supplement*, (18), 173183.
- Dreiss, S. J., and L. D. Anderson (1985), Estimating vertical soil moisture flux at a land treatment site, *Ground Water*, 23(4), 503–511.
- Droogers, P., and R. G. Allen (2002), Estimating reference evapotranspiration under inaccurate data conditions, *Irrigation and Drainage Systems*, 16(1), 33–45.
- Dugan, J.T., and R.B. Zelt, (2000), Simulations and analysis of soil-water conditions in the Great Plains and adjacent areas, Central United States, 1951-80. USGS Water-Supply Paper 2427.
- Flint, A. L., G. S. Ellett, K. M. Calissendorff, and others (2002), Calibration and temperature correction of heat dissipation matric potential sensors, *Soil Science Society of America Journal*, 66(5), 1439.
- Flury, M., H. Flühler, W. A. Jury, and J. Leuenberger (1994), Susceptibility of soils to preferential flow of water: A field study, *Water Resources Research*, 30(7), 1945–1954.

- Gardner, C. S., J. M. Greene, M. D. Kruskal, and R. M. Miura (1967), Method for Solving the Korteweg-deVries Equation, *Phys. Rev. Lett.*, 19(19), 1095, doi:10.1103/PhysRevLett.19.1095.
- Gee, G. W., M. J. Fayer, M. L. Rockhold, P. J. Wierenga, M. H. Young, and B. J. Andraski (1994), Variations in water balance and recharge potential at three western desert sites, *Soil Science Society of America Journal;(United States)*, 58(1).
- Glass, R. J., and T. S. Steenhuis (1984), Factors influencing infiltration flow instability and movement of toxics in layered sandy soils, *Paper-American Society of Agricultural Engineers (USA); Microfiche collection*.
- Glass, R. J., J. Y. Parlange, and T. S. Steenhuis (1987), Water infiltration in layered soils where a fine textured layer overlays a coarse sand, *Infiltration Development and Application*, 66–81.
- Glass, R. J., J. Y. Parlange, and T. S. Steenhuis (1989a), Wetting front instability: 1. Theoretical discussion and dimensional analysis, *Water Resources Research*, 25(6), 1187–1194.
- Glass, R. J., T. S. Steenhuis, and J. Parlange (1989b), Wetting front instability: 2. Experimental determination of relationships between system parameters and two-dimensional unstable flow field behavior in initially dry porous media, *Water Resour. Res.*, 25(6), PP. 1195-1207, doi:198910.1029/WR025i006p01195.
- Glass, R. J., T. S. Steenhuis, and J. Y. Parlange (1989c), Mechanism for finger persistence in homogeneous, unsaturated, porous media: Theory and verification, *Soil Science*, 148(1), 60.
- Gleick, P.H., H. Cooley, M. Cohen, M. Morikawa, J. Morrison, and M. Palaniappan (2009), *The World's Water: The Biennial Report on Freshwater Resources*, 401 pp., edited by T. Baldwin, Island Press, Washington, DC.
- Gurdak, J. J., R. T. Hanson, P. B. McMahon, B. W. Bruce, J. E. McCray, G. D. Thyne, and R. C. Reedy (2007), Climate variability controls on unsaturated water and chemical movement, High Plains Aquifer, USA, *Vadose Zone Journal*, 6(3), 533.

- Gurdak, J. J., M. A. Walvoord, and P. B. McMahon (2008), Susceptibility to Enhanced Chemical Migration from Depression-Focused Preferential Flow, High Plains Aquifer, *Vadose Zone Journal*, 7(4), 1218-1230, doi:10.2136/vzj2007.0145.
- Gurdak, J. J., and C. D. Roe (2010), Review: Recharge rates and chemistry beneath playas of the High Plains aquifer, USA, *Hydrogeol J*, 18(8), 1747-1772, doi:10.1007/s10040-010-0672-3.
- Gutenag, E.D., Heimes, F.J., Krothe, N.C., Luckey, R.R., and J.B. Weeks (1984), Regional aquifer-system analysis of the High Plains aquifer in parts of Colorado, Kansas, Nebraska, New Mexico, Oklahoma, South Dakota, Texas, and Wyoming-Geohydrology. United States Geological Survey Professional Paper 1400-B.
- Hargreaves, G. H., and Z. A. Samani (1982), Estimating potential evapotranspiration, *Journal of the Irrigation and Drainage Division*, 108(3), 225–230.
- Hartsough, P., S. W. Tyler, J. Sterling, and M. Walvoord (2001), A 14.5 kyr record of nitrogen flux from desert soil profiles as inferred from vadose zone pore waters, *Geophys. Res. Lett*, 28, 2955–2958.
- Hendrickx, J.M.H., and M. Flury. (2001). Uniform and preferential flow mechanisms in the vadose zone. p. 19–188. *In* Conceptual models of flow and Transport in the fractured vadose zone. Natl. Acad. Press, Washington, DC.
- Hill, D. E., and J.-Y Parlange (1972), Wetting Front Instability in Layered Soils1, *Soil Science Society of America Journal*, 36(5), 697.
- Hillel, D. (1987), Unstable flow in layered soils: A review, *Hydrological Processes*, 1(2), 143–147.
- HPRCC (2010), High Plains Regional Climate Center (HPRCC), Available at <http://www.hprcc.unl.edu/> (verified November 2010), High Plains Regional Climate Center, Lincoln, NE.
- IAEA. (2001). Isotope Based Assessment of Groundwater Renewal in Water Scarce Regions, IAEA TecDoc 1246. IAEA: Vienna; 273 p.

- Izbicki, J. A. (2007), Ground-water recharge from small intermittent streams in the western Mojave Desert, California, *U. S. Geological Survey Professional Paper*, 157-184.
- Jarvis, N., (1998), Modeling the impact of preferential flow on nonpoint source pollution, in *Physical Non-Equilibrium in Soils: Modeling and Application*, edited by H.M. Selim, and L. Ma, pp. 195–221, CRC Press, Boca Raton, Fla.
- Jury, W. A. (1982), Simulation of solute transport using a transfer function model, *Water Resour. Res.*, 18(2), PP. 363-368, doi:198210.1029/WR018i002p00363.
- Jury, W. A., Z. Wang, and A. Tuli (2003), A conceptual model of unstable flow in unsaturated soil during redistribution, *Vadose Zone Journal*, 2(1), 61.
- Lebeau, M., and J. M. Konrad (2010), A new capillary and thin film flow model for predicting the hydraulic conductivity of unsaturated porous media, *Water Resources Research*, 46(12), W12554.
- Martinez-Cob, A., and M. Tejero-Juste (2004), A wind based qualitative calibration of the Hargreaves ET₀ estimation equation in semiarid regions. *Agricultural Water Management*, 64, 251–264.
- Maupin, M.A., and N.L., Barber (2005), Estimated withdrawals from principal aquifers in the United States, 2000: U.S. Geological Survey Circular 1279, 46 p.
- McMahon, P. B., K. F. Dennehy, R. L. Michel, M. A. Sophocleous, K. M. Ellett, and D. B. Hurlbut (2003), Water Movement Through Thick Unsaturated Zones Overlying the Central High Plains Aquifer, Southwestern Kansas, 2000-2001. *Water-Resources Investigations Report 03-4171.*, 1-32 p.
- McMahon, P. B., K. F. Dennehy, B. W. Bruce, J. K. Boehlke, R. L. Michel, J. J. Gurdak, and D. B. Hurlbut (2006), Storage and transit time of chemicals in thick unsaturated zones under rangeland and irrigated cropland, High Plains, United States, *Water Resour. Res.*, 42, W03413, doi:10.1029/2005WR004417.

- McMahon, P.B., K.F. Dennehy, B.W. Bruce, J.J. Gurdak, and S.L. Qi (2007), Water-quality assessment of the High Plains aquifer, 1999-2004: *U.S. Geological Survey Professional Paper 1749*, 136 p.
- National Land Cover Database (2001), accessed April 5, 2011, at http://www.mrlc.gov/mrlc2k_nlcd.asp.
- Nativ, R. (1992), Recharge into Southern High Plains aquifer—possible mechanisms, unresolved questions, *Environmental Geology*, 19(1), 21–32.
- Nimmo, J. R., D. A. Stonestrom, and K. C. Akstin (1994), The feasibility of recharge rate determinations using the steady-state centrifuge method, *Soil Science Society of America Journal*, 58(1), 49–49.
- Nimmo, J. R. (2007), Simple predictions of maximum transport rate in unsaturated soil and rock, *Water Resour. Res.*, 43(5), W05426.
- Nimmo, J. R. (2010), Theory for Source-Responsive and Free-Surface Film Modeling of Unsaturated Flow, *Vadose Zone Journal*, 9(2), 295-306, doi:10.2136/vzj2009.0085.
- NOAA (2010), United States Historical Climatology Network (USHCN). Available at <http://www.ncdc.noaa.gov/oa/climate/research/ushcn/ushcn.html> (verified November 2010). National Climate Data Center, NOAA, Asheville, NC.
- Phillips, F. M. (1994), Environmental tracers for water movement in desert soils of the American Southwest, *Soil Science Society of America Journal*, 58(1), 15–24.
- Phillips, F.M., M.A. Walvoord, and E.E. Small (2004), Effects of environmental change on groundwater recharge in the desert southwest. In *Groundwater Recharge in a Desert Environment: The Southwestern United States*, Water Science and Application 9, ed. J.F. Hogan, F.M. Phillips, and B.R. Scanlon, 273-294. American Geophysical Union.
- Qi, S.L., Konduris, A., Litke, D.W., and Dupree, J., 2002, Classification of irrigated land using satellite imagery, the High Plains aquifer, nominal data 1992: U.S. Geological Survey Water-Resources Investigations Report 02–4236, 31 p.

- Rezanezhad, F., H. J. Vogel, and K. Roth (2006), Experimental study of fingered flow through initially dry sand, *Hydrology and Earth System Sciences Discussions*, 3(4), 2595–2620.
- Robinson, D. A., S. B. Jones, J. M. Wraith, D. Or, and S. P. Friedman (2003), A review of advances in dielectric and electrical conductivity measurement in soils using time domain reflectometry, *Vadose Zone Journal*, 2(4), 444.
- Rimon, Y., O. Dahan, R. Nativ, and S. Geyer (2007), Water percolation through the deep vadose zone and groundwater recharge: Preliminary results based on a new vadose zone monitoring system, *Water Resour. Res.*, 43, 12 PP., doi:200710.1029/2006WR004855.
- Rimon, Y., R. Nativ, and O. Dahan (2011), Physical and Chemical Evidence for Pore-Scale Dual-Domain Flow in the Vadose Zone, *Vadose Zone Journal*, 10(1), 322-331, doi:10.2136/vzj2009.0113.
- Ritsema, C. J., L. W. Dekker, J. M. H. Hendrickx, and W. Hamminga (1993), Preferential flow mechanism in a water repellent sandy soil, *Water Resour. Res.*, 29(7), PP. 2183-2193, doi:199310.1029/93WR00394.
- Ritsema, C. J., and L. W. Dekker (1994), How water moves in a water repellent sandy soil: 2. Dynamics of fingered flow, *Water Resour. Res.*, 30(9), PP. 2519-2531, doi:199410.1029/94WR00750.
- Ritsema, C. J., L. W. Dekker, J. L. Nieber, and T. S. Steenhuis (1998), Modeling and field evidence of finger formation and finger recurrence in a water repellent sandy soil, *Water Resources Research*, 34(4), 555–567.
- Seyfried, M. S., S. Schwinning, M. A. Walvoord, W. T. Pockman, B. D. Newman, R. B. Jackson, and F. M. Phillips (2005), Ecohydrological control of deep drainage in arid and semiarid regions, *Ecology*, 86(2), 277-287, doi:10.1890/03-0568.
- Scanlon, B. R., S. W. Tyler, and P. J. Wierenga (1997), Hydrologic issues in arid, unsaturated systems and implications for contaminant transport, *Reviews of Geophysics*, 35(4), 461–490.

- Scanlon, B. R., and R. S. Goldsmith (1997), Field study of spatial variability in unsaturated flow beneath and adjacent to playas, *Water Resources Research*, 33(10), 2239–2252.
- Scanlon, B. R., R. P. Langford, and R. S. Goldsmith (1999), Relationship between geomorphic settings and unsaturated flow in an arid setting, *Water Resources Research*, 35(4), 983–999.
- Scanlon, B. R. (2000), Uncertainties in estimating water fluxes and residence times using environmental tracers in an arid unsaturated zone, *Water Resources Research*, 36(2), 395–409.
- Scanlon, B. R., R. W. Healy, and P. G. Cook (2002), Choosing appropriate techniques for quantifying groundwater recharge, *Hydrogeology Journal*, 10(1), 18–39.
- Scanlon, B. R., K. Keese, R. C. Reedy, J. Simunek, and B. J. Andraski (2003), Variations in flow and transport in thick desert vadose zones in response to palaeoclimatic forcing (0-90 kyr): field measurements, modeling and uncertainties, *Water Resources Research*, 39(7), 1179–1196.
- Scanlon, B. R., R. C. Reedy, D. A. Stonestrom, D. E. Prudic, and K. F. Dennehy (2005), Impact of land use and land cover change on groundwater recharge and quality in the southwestern US, *Global Change Biol*, 11(10), 1577-1593, doi:10.1111/j.1365-2486.2005.01026.x.
- Scanlon, B. R., K. E. Keese, A. L. Flint, L. E. Flint, C. B. Gaye, W. M. Edmunds, and I. Simmers (2006), Global synthesis of groundwater recharge in semiarid and arid regions, *Hydrol. Process.*, 20(15), 3335-3370, doi:10.1002/hyp.6335.
- Skopp, J., (1981), Comments on “Micro-meso-and macroporosity of soil”, *Soil Sci. Soc. Am. J.*, 45, 1246.
- Small, E.E., (2005), Climatic controls on diffuse groundwater recharge in semiarid environments of the southwestern United States. *Water Resour. Res.*, 41, WO4012, doi:10.1029/2004WR003193.

- Smith, G.I., I. Friedman, J.D. Gleason, and A. Warden (1992), Stable isotope composition of waters in southeastern California : Part 2, Groundwaters and their relation to modern precipitation, *J. Geophysical Res.*, 97, 5813-5824.
- Stephens, D.B., (1996) *Vadose Zone Hydrology*, A.F. Lewis, Boca Raton, Fla.,
- Szilagyi, J., F. E. Harvey, and J. F. Ayers (2003), Regional estimation of base recharge to ground water using water balance and a base-flow index, *Ground Water*, 41(4), 504–513.
- Szilagyi, J., and J. Jozsa (2009), Estimating spatially distributed monthly evapotranspiration rates by linear transformations of MODIS daytime land surface temperature data, *Hydrology and Earth System Sciences*, 13(5), 629–637.
- Tindall, J.A., J.R. Kunkel, and R.A. McConnin (Ed.) (1999), *Unsaturated Zone Hydrology for Scientists and Engineers*, 624 pp., Prentice-Hall, Inc., New Jersey.
- Thatcher, L. L. (1962), The distribution of tritium fallout in precipitation over North America, *Bull. Int. Assoc. Sei. Hydrol*, 7(2), 48.
- United Nations (2004), Department of Economic and Social Affairs/Population Division, *World Population to 2300*; 4.
- Van Genuchten, M.Th., F.J. Leij, and S.R. Yates. (1991) The RETC code for quantifying the hydraulic functions of unsaturated soils. USEPA, Washington, DC.
- Walvoord, M. A., M. A. Plummer, F. M. Phillips, and A. V. Wolfsberg (2002), Deep arid system hydrodynamics: 1. Equilibrium states and response times in thick desert vadose zones, *Water Resour. Res.*, 38(12), 1308.
- Walvoord, M.A., Phillips, F.M., Stonestrom, D.A., Evans, R.D., Hartsough, P.C., Newman, B.D., and R.G. Sriegl (2003), A reservoir of nitrate beneath desert soils. *Science*, 302(5647), 1021-1024.

- Walvoord, M.A., and B.R. Scanlon (2004), Hydrologic processes in deep vadose zones in interdrainage arid environments. In *Groundwater Recharge in a Desert Environment: The Southwestern United States*, Water Science and Application 9, ed. J.F. Hogan, F.M. Phillips, and B.R. Scanlon, 15-28. American Geophysical Union.
- Wang, Z., L. Wu, T. Harter, J. Lu, and W. A. Jury (2003), A field study of unstable preferential flow during soil water redistribution, *Water Resour. Res.*, 39(4), 1075.
- Wellings, S. R., and J. P. Bell (1982), Physical controls of water movement in the unsaturated zone, *Quarterly Journal of Engineering Geology and Hydrogeology*, 15(3), 235.
- WHO. (2003), *Right to Water. Health and Human Rights Publication Series No. 3*, World Health Organization: Geneva, Switzerland; 44.
- Wood, W. W., K. A. Rainwater, and D. B. Thompson (1997), Quantifying Macropore Recharge: Examples from a Semi-Arid Area, *Ground Water*, 35(6), 1097–1106.
- Wood, W. W. (1999), Comment on “Field study of spatial variability in unsaturated flow beneath and adjacent to playas” by Bridget R. Scanlon and Richard S. Goldsmith, *Water Resources Research*, 35(2), 601–601.

Table 1) IMP fronts #1–4 with arrival date of wetting front at each HDP and estimated water fluxes between 0.5 m and the final depth of propagation.

Front	1	2	3	4
Depth (m)	2007	2008	Late 2008	2009/10
0.5	2/22/2007	4/12/2008	10/21/2008	10/4/2009
1.5	3/10/2007	5/5/2008	11/1/2008	11/9/2009
2.5	3/25/2007	5/15/2008	3/17/2009	11/29/2009
5.0	5/19/2007	6/16/2008	5/29/2009	4/27/2010
6.4	6/19/2007	7/25/2008	7/18/2009	5/16/2010
7.9	7/15/2007	8/11/2008	8/15/2009	6/12/2010
9.5	7/31/2007	9/3/2008	9/20/2009	6/26/2010
17.0	10/12/2007			9/13/2010
20.0	12/8/2007			
23.0	3/16/2008			
Days	387	144	333	344
Total Potential	0.83	15.52	15.49	15.66
θ	0.2343	0.2532	0.2526	0.2555
q (mm/d) =	13.62	15.83	6.83	12.63
q (mm/yr)=	4972.06	5776.13	2491.86	4608.66
velocity m/d	0.0581	0.0625	0.0270	0.0262
error +/- θ	0.0469	0.0506	0.0505	0.0511
q +/- =	994.41	1155.23	498.37	921.73

Table 2) CNG fronts #1–5 with wetting front arrival date at each HDP and estimated water fluxes for traveltime between 0.5 m and the final depth of propagation.

Front #	1	2	3	4	5
Depth (m)	2006-07	2008	2008-09	2009	2009-10
0.5	12/20/2006	7/18/2008	10/15/2008	4/7/2009	10/27/2009
1.5	1/2/2007	8/23/2008	10/21/2008	5/5/2009	4/4/2010
2.5	1/28/2007		11/27/2008	5/26/2009	4/25/2010
3.5	2/25/2007		1/15/2009	6/29/2009	
5.0	3/6/2007			12/25/2009	
7.3				2/13/2010	
Days	67	36	91	213	180
Total Potential	44.31	43.18	41.16	40.49	46.19
θ	0.2828	0.1827	0.1594	0.2880	0.3613
q (mm/d)=	12.66	5.08	7.88	9.19	4.01
q (mm/yr)=	4621.88	1852.38	2877.08	3355.94	1465.27
velocity m/d	0.0448	0.0278	0.0440	0.0319	0.0111
20% error on Theta	0.0566	0.0365	0.0319	0.0576	0.0723
q +/- =	924.38	370.48	959.03	671.19	293.05

Table 3) IMP Front #1- Final time step (570 days) indicating the change in storage below the ZFP reached a depth of 23.0 m (time steps 373 and 423 days have the same range of storage increase).

		2/22/2007	9/14/2008				
Depth of Increase (m)	Depth, m	0	0				
23.0		Day 1	Day 570	s1	s2	ΔS-below ZFP	ΔS-above ZFP
	0.5	0.3776	0.1722	0.1888	0.0861		-0.1027
	1.5	0.3694	0.3713	0.3735	0.2718		-0.1018
	2.4	0.3587	0.3597	0.3276	0.3290	0.0013	
	2.5	0.3784	0.3808	0.0369	0.0370	0.0002	
	5.0	0.3737	0.3775	0.9401	0.9479	0.0078	
	6.4	0.0133	0.0171	0.2709	0.2762	0.0053	
	7.9	0.2498	0.2689	0.1973	0.2145	0.0172	
	9.5	0.2444	0.2540	0.3954	0.4183	0.0230	
	17.0	0.2617	0.2732	1.8979	1.9770	0.0791	
	20.0	0.2591	0.2624	0.7812	0.8034	0.0222	
	23.0	0.2332	0.2394	0.7385	0.7527	0.0143	
	Storage Increase (m)	PREC (m)	HARG (m)	COMBO (m)			
	0.1703	0.4270	0.1840	0.0890			
Percent Difference				47.73			
(Precipitation-ET)-ΔS		0.2567	0.0137	-0.0813			

Table 4) IMP front #1-Calculations of precipitation, precipitation-ET using the HARG equation, and The COMBO method. Bold numbers are estimate of available precipitation.

HARG (Hargreaves and Samani, 1982)							
DATE	prec (mm)	sum (mm)	sum (m)	ET (mm/mo)	Prec-ET (mm)	sum (mm)	sum (m)
200612	39.6240			10.0862	29.5378		
200701	4.3180			7.1310	-2.8130		
200702	17.2720	61.2140	0.0612	10.6649	6.6071	36.1449	0.0361
200703	31.7500			36.0767	-4.3267		
200704	72.8980	165.8620	0.1659	41.3265	31.5715	67.7164	0.0677
200705	99.8220			67.5341	32.2879		
200706	161.2900	426.9740	0.4270	77.3327	83.9573	183.9615	0.1840
COMBO (Szilagyi and Jozsa (2009) plus Dugan and Zelt (2000))							
DATE	ET (mm)	Prec-ET (mm)	sum (mm)	sum (m)			
200612	0.0000	39.6240					
200701	0.0000	4.3180					
200702	0.0000	17.2720	61.2140	0.0612			
200703	18.6000	13.1500					
200704	76.4800	-3.5820	74.3640	0.0744			
200705	104.2400	-4.4180					
200706	142.4400	18.8500	89.6320	0.0896			
DATE	ET (mm)	prec-ET (mm)	sum (mm)	sum (m)			

Table 5) IMP Front #1- The final three time steps have sufficient available precipitation from the HARG method and precipitation alone.

373 days	Storage Increase (m) 0.1906	PREC (m) 0.4270	HARG (m) 0.1840	COMBO (m) 0.0896
Percent Difference			3.44	52.98
(Precipitation-ET)-ΔS		0.2364	-0.0066	-0.1010
423 days	Storage Increase (m) 0.1889	PREC (m) 0.4270	HARG (m) 0.1840	COMBO (m) 0.0896
Percent Difference				52.58
(Precipitation-ET)-ΔS		0.2381	-0.0049	-0.0993
570 days	Storage Increase (m) 0.1703	PREC (m) 0.4270	HARG (m) 0.1840	COMBO (m) 0.0890
Percent Difference				47.73
(Precipitation-ET)-ΔS		0.2567	0.0137	-0.0813

Table 6) CNG Front #1- Final time step indicates there is enough available precipitation to account for the change in storage. Depth of increase pertains to final depth of observed increase in total potential.

		12/20/2006	8/10/2007				
Depth of increase (m)	Depth, m	θ	θ				
5.0		Day 1	Day 233	s1	s2	ΔS -below ZFP	ΔS -above ZFP
	0.5	0.3472	0.2410	0.1736	0.1205		-0.0531
	1.5	0.1789	0.1632	0.2631	0.2021		-0.0610
	2.5	0.3150	0.3610	0.2470	0.2621		0.0152
	3.5	0.2600	0.3425	0.2875	0.3518	0.0643	
	5.0	0.1429	0.1585	0.3022	0.3758	0.0736	
	7.3	0.2830	0.2860	0.4898	0.5112	0.0214	
	9.7	0.2950	0.2937	0.6936	0.6956	0.0020	
	Storage Increase (m)		HARG (m)	COMBO (m)			
	0.1592	PREC (m)					
		0.3147	0.1519	0.1590			
Percent Difference (Precipitation-ET)- ΔS			4.59	1.35			
		0.1555	-0.0073	-0.0002			

Table 7) CNG Front #1- Amount of precipitation and ET estimates from October 2006 through May 2007, bold numbers indicate the values used for comparison with change in storage calculations.

HARG (Hargreaves and Samani, 1982)							
Date	Precipitation (mm)	sum (mm)	sum (m)	ET (mm)	Prec-ET (mm)	sum (mm)	sum (m)
10/06	43.9420			33.7998	10.1422		
11/06	0.0000			15.7050	-15.7050		
12/06	129.7940	173.7360	0.1737	11.5553	118.2387	128.3809	0.1284
1/07	8.6360	182.3720		9.4316	-0.7956	128.3809	0.1284
2/07	4.0640	186.4360		17.6321	-13.5681	128.3809	0.1284
3/07	37.0840	223.5200		36.4457	0.6383	129.0192	0.1290
4/07	64.2620	287.7820		41.4168	22.8452	151.8644	0.1519
5/07	26.9240	314.7060	0.3147	65.3872	-38.4632		
COMBO (Szilagyi and Jozsa (2009) plus Dugan and Zelt (2000))							
Date	ET (mm)	Prec-ET (mm)	sum (mm)	sum (m)			
10/06	57.7900	-13.8480					
11/06	11.4800	-11.4800					
12/06	0.0000	129.7940	129.7940	0.1298			
1/07	0.0000	8.6360	138.4300	0.1380			
2/07	0.0000	4.0640					
3/07	20.5900	16.4940					
4/07	84.6300	-20.3680					
5/07	115.3400	-88.4160	158.9880	0.1590			

Table 8) IMP Front #2 had an estimated increase in storage of ~0.0143 between 2.5 m and 9.5 m. Increase in storage above 2.4 m is assumed to be from recent precipitation events not included in the change in storage at depth. Depth of increase is observed increase in total potential.

		4/11/2008	12/21/2008				
Depth of Increase	Depth, m	θ	θ				
9.5		Day 1	Day 234	s1	s2	DS-below ZFP	DS-above ZFP
	0.5	0.1797	0.3282	0.0899	0.1641	0.0743	
	1.5	0.3787	0.3779	0.2792	0.3531	0.0739	
	2.4	0.3581	0.3637	0.3316	0.3337	0.0022	
	2.5	0.3806	0.3806	0.0369	0.0372	0.0003	
	5.0	0.3758	0.3774	0.9455	0.9475	0.0020	
	6.4	0.0148	0.0171	0.2734	0.2762	0.0027	
	7.9	0.2689	0.2736	0.2128	0.2180	0.0053	
	9.5	0.2560	0.2564	0.4199	0.4240	0.0041	
	17.0	0.2765	0.2723	1.9969	1.9826	-0.0143	
	20.0	0.2630	0.2630	0.8093	0.8030	-0.0063	
	23.0	0.2353	0.2392	0.7475	0.7533	0.0058	
	Storage Increase (m)	PREC (m)	HARG (m)	COMBO (m)			
	0.0143	0.4115	0.0762	0.0139			
Percent Difference				0.0307			
(Precipitation-ET)- ΔS		0.3972	0.0619	-0.0004			

Table 9) IMP Front #2 available precipitation and ET estimates.

HARG (Hargreaves and Samani, 1982)							
DATE	prec (mm)	sum (mm)	sum (m)	ET (mm)	Prec-ET (mm)	sum (mm)	sum (m)
200801	0.5080			10.4342	-9.9262		
200802	3.8100			20.3178	-16.5078		
200803	15.2400			34.7509	-19.5109		
200804	64.2620			55.8260	8.4360		
200805	113.7920	197.6120		63.7492	50.0428	58.4788	0.0585
200806	83.5660	261.6200	.0.2616	87.0229	-3.4569	58.4788	0.0585
200807	59.1820	320.8020		102.0469	-42.8649	58.4788	0.0585
200808	90.6780	411.4800	0.4115	72.9923	17.6857	76.1645	0.0762
COMBO (Szilagyi and Jozsa (2009) plus Dugan and Zelt (2000))							
DATE	ET (mm)	Prec-ET (mm)	sum (mm)	sum (m)			
200801	0.0000	0.5080					
200802	0.0000	3.8100					
200803	18.6000	-3.3600					
200804	76.4800	-12.2180					
200805	104.2400	9.5520	13.8700	0.0139			
200806	142.4400	-58.8740					
200807	172.4800	-					
200808	124.29	-33.612	13.87	0.0139			

Table 10) IMP Front #3- had an increase in storage to a depth of 6.4 m. Total potential was observed to increase to a depth of 9.5 m.

		10/21/2008	1/16/2010				
Depth of Increase (m)	Depth, m	θ	θ				
9.5		Day 1	Day 451	s1	s2	ΔS -below ZFP	ΔS -above ZFP
	0.5	0.1790	0.3674	0.0895	0.1837	0.0942	
	1.5	0.3734	0.3790	0.2762	0.3732	0.0970	
	2.4	0.3605	0.3645	0.3303	0.3346	0.0043	
	2.5	0.3807	0.3807	0.0371	0.0373	0.0002	
	5.0	0.3777	0.3783	0.9480	0.9488	0.0008	
	6.4	0.0168	0.0169	0.2762	0.2766	0.0005	
	7.9	0.2707	0.2694	0.2156	0.2147	-0.0009	
	9.5	0.2551	0.2543	0.4206	0.4190	-0.0017	
	17.0	0.2727	0.2711	1.9793	1.9703	-0.0090	
	20.0	0.2624	0.2618	0.8027	0.7994	-0.0033	
	23.0	0.2396	0.2382	0.7530	0.7500	-0.0030	
	Storage Increase (m)	PREC (m)	HARG (m)	COMBO (m)			
	0.1970	0.4229	0.1145	0.1133			
Percent Difference			41.87	42.48			
(Precipitation-ET)- ΔS		0.2259	-0.0825	-0.0837			

Table 11) IMP Front #3 available precipitation and ET estimates.

HARG (Hargreaves and Samani, 1982)							
DATE	Prec (mm)	sum (mm)	sum (m)	ET (mm/mo)	Prec-ET (mm/mo)	sum (mm)	sum (m)
200808	90.6780			72.9923	17.6857		
200809	52.5780			62.6426	-10.0646		
200810	66.0400			35.6530	30.3870		
200811	22.8600			18.8281	4.0319		
200812	5.8420			9.7308	-3.8888		
200901	5.8420			15.2674	-9.4254		
200902	29.4640			23.7423	5.7217		
200903	6.8580			38.2398	-31.3818		
200904	0.0000			46.5795	-46.5795		
200905	75.1840	355.3460	0.355346	68.8148	6.3692	64.1955	0.0642
200906	0.0000			80.1260	-80.1260		
200907	0.0000			89.2732	-89.2732		
200908	49.2760	404.6220	0.404622	85.1678	-35.8918	64.1955	0.0642
COMBO (Szilagyi and Jozsa (2009) plus Dugan and Zelt (2000))							
DATE	ET (mm)	Prec-ET (mm)	sum (mm)	sum (m)			
200808	124.2900	-33.6120					
200809	84.6400	-32.0620					
200810	52.2300	13.8100					
200811	10.3700	12.4900					
200812	0.0000	5.8420					
200901	0.0000	5.8420					
200902	0.0000	29.4640					
200903	18.6000	-11.7420					
200904	76.4800	-76.4800					

200905	104.2400	-29.0560	67.4480	0.0674			
200906	142.4400	-142.4400					
200907	172.4800	-172.4800					
200908	124.2900	-75.0140	67.4480	0.0674			

Table 12) IMP Front #4- Observed total potential increase reached a depth of 17.0 m. Increase in storage reached a depth of 23.0 m. 20.0–23.0 m increase could be drainage increase.

		10/4/2009	11/5/2010				
Depth of Increase (m)	Depth, m	θ	θ				
17.0		Day 1	Day 396	s1	s2	ΔS -below ZFP	ΔS -above ZFP
	0.5	0.2868	0.3392	0.1434	0.1696	0.0262	
	1.5	0.3713	0.3784	0.3291	0.3588	0.0298	
	2.4	0.3614	0.3629	0.3297	0.3336	0.0039	
	2.5	0.3807	0.3807	0.0371	0.0372	0.0001	
	5.0	0.3777	0.3755	0.9480	0.9453	-0.0028	
	6.4	0.0164	0.0166	0.2759	0.2745	-0.0014	
	7.9	0.2679	0.2785	0.2132	0.2213	0.0081	
	9.5	0.2527	0.2644	0.4165	0.4343	0.0178	
	17.0	0.2713	0.2765	1.9650	2.0284	0.0634	
	20.0	0.2615	0.2623	0.7992	0.8082	0.0090	
	23.0	0.2383	0.2387	0.7497	0.7515	0.0018	
	Storage Increase (m)	PREC (m)	HARG (m)	COMBO (m)			
	0.1559	0.5964	0.2383	0.1492			
Percent Difference				0.0427			
(Precipitation-ET)- ΔS		0.4000	0.0419	-0.0472			

Table 13) IMP Front #4 precipitation and ET estimates.

				HARG (<i>Hargreaves and Samani, 1982</i>)			
DATE	Prec (mm)	sum (mm)	sum (m)	ET (mm)	Prec-ET (mm)	sum (mm)	sum (m)
200908	49.2760			85.1678	-35.8918		
200909	57.4040			56.8749	0.5291		
200910	87.8840			22.9998	64.8842		
200911	6.0960			21.1672	-15.0712		
200912	10.1600			7.5851	2.5749		
201001	2.2860			11.1055	-8.8195		
201002	14.9860	228.0920	0.2281	14.7028	0.2832	68.2714	0.0683
201003	49.7840	277.8760	0.2779	33.3865	16.3975	84.6688	0.0847
201004	76.7080			49.4740	27.2340		
201005	44.7040	399.2880	0.3993	66.8016	-22.0976	111.9029	0.1119
201006	197.1040	596.3920	0.5964	91.8002	105.3038	217.2067	0.2172
COMBO (<i>Szilagyi and Jozsa (2009) plus Dugan and Zelt (2000)</i>)							
DATE	ET (mm)	Prec-ET (mm)	sum (mm)	sum (m)			
200908	124.2900	-75.0140					
200909	84.6400	-27.2360					
200910	52.2300	35.6540					
200911	10.3700	-4.2740					
200912	0.0000	10.1600					

201001	0.0000	2.2860					
201002	0.0000	14.9860	63.0860	0.0631			
201003	18.6000	31.1840	84.1100	0.0841			
201004	76.4800	0.2280					
201005	104.2400	-59.5360	94.4980	0.0945			
201006	142.4400	54.6640	149.1620	0.1492			

Table 14) IMP Front #4- Estimates of HARG and COMBO are within the estimated 10% error range.

Time Step 236 days	Storage Increase (m)	PREC (m)	HARG (m)	COMBO (m)
	0.1182	0.3993	0.1119	0.0945
Percent Difference (Precipitation-ET)- ΔS			5.30	20.03
		0.2811	-0.0063	-0.0237
Time step 308 days	Storage Increase (m)	PREC (m)	HARG (m)	COMBO (m)
	0.1612	0.5964	0.2127	0.1492
Percent Difference (Precipitation-ET)- ΔS				7.45
		0.4352	0.0515	-0.0120
Time step 396 days	Storage Increase (m)	PREC (m)	HARG (m)	COMBO (m)
	0.1559	0.5964	0.2383	0.1492
Percent Difference (Precipitation-ET)- ΔS				4.27
		0.4000	0.0419	-0.0472

Table 15) CNG Front #2 - All three methods fail to account for the estimated change in storage from depth 0.5 m to 2.5 m.

		7/18/2008	9/7/2008				
Depth of increase (m)	Depth, m	θ	θ				
0.5-1.5		Day 1	Day 51	s1	s2	ΔS -below ZFP	ΔS -above ZFP
	0.5	0.2426	0.3615	0.1213	0.1808	0.0595	
	1.5	0.1568	0.3739	0.1997	0.3677	0.1680	
	2.5	0.3127	0.3099	0.2348	0.3419	0.1072	
	3.5	0.2156	0.2000	0.2642	0.2550	-0.0092	
	5.0	0.1532	0.1488	0.2766	0.2616	-0.0150	
	7.3	0.2890	0.2860	0.5085	0.5000	-0.0085	
	9.7	0.2924	0.2911	0.6977	0.6925	-0.0052	
	Storage Increase (m)	PREC (m)	HARG (m)	COMBO (m)			
	0.3346	0.1821	0.0634	0.0000			
Percent Difference		0.4558	0.8105	1.0000			
(Precipitation-ET)-ΔS		-0.1263	-0.2590	-0.3224			

Table 16) CNG Front #3- Final time step of 166 days. The available precipitation alone and from the HARG estimate were sufficient to account for the change in storage. Depth of increase pertains to the observed increase in total potential.

		10/15/2008	3/31/2009				
Depth of increase (m)	Depth, m	θ	θ				
3.5		Day 1	Day 166	s1	s2	ΔS -below ZFP	ΔS -above ZFP
	0.5	0.3504	0.3680	0.1752	0.1840	0.0088	
	1.5	0.3603	0.3720	0.3554	0.3700	0.0147	
	2.5	0.3113	0.3785	0.3358	0.3753	0.0395	
	3.5	0.1981	0.2220	0.2547	0.3003	0.0456	
	5.0	0.1500	0.1595	0.2611	0.2861	0.0251	
	7.3	0.2840	0.2880	0.4991	0.5146	0.0155	
	9.7	0.2911	0.2916	0.6901	0.6955	0.0054	
	Storage Increase (m)	PREC (m)	HARG (m)	COMBO (m)			
	0.1544	0.3683	0.1660	0.0175			
Percent Difference				0.8866			
(Precipitation-ET)-ΔS		0.2139	0.0116	-0.1369			

Table 17) CNG Front #2 and #3-Precipitation data and ET estimates from HARG method and COMBO method, bold values used in comparison with change in storage at the four time steps calculated between the two fronts.

HARG (<i>Hargreaves and Samani, 1982</i>)							
Date	prec	sum (mm)	sum (m)	ET	Prec-ET	sum (mm)	sum (m)
200806	15.4940			90.6074	-75.1134		
200807	42.4180			82.8719	-40.4539		
200808	124.2060	182.1180	0.1821	60.7564	63.4496	63.4496	0.0634
200809	13.9700	196.0880	0.1961	48.1334	-34.1634	63.4496	0.0634
200810	132.0800			29.5594	102.5206		
200811	2.0320			18.0482	-16.0162		
200812	3.5560	333.7560	0.3338	11.0776	-7.5216	165.9702	0.1660
200901	0.5080			13.9908	-13.4828		
200902	10.4140			24.4795	-14.0655		
200903	23.6220	368.3000	0.3683	33.4701	-9.8481	165.9702	0.1660
COMBO (<i>Szilagyi and Jozsa (2009) plus Dugan and Zelt (2000)</i>)							
Date	ET (mm)	Prec-ET (mm)	sum (mm)	sum (m)			
200806	157.6100	-					
200807	190.8600	-					
200808	137.5400	-13.3340					
200809	93.6600	-79.6900	0.0000	0.0000			
200810	57.7900	74.2900					
200811	11.4800	-9.4480					
200812	0.0000	3.5560	77.8460	0.0778			
200901	0.0000	0.5080					

200902	0.0000	10.4140					
200903	20.5900	3.0320	17.5100	0.0175			

Table 18) CNG Front #4 the depth of total potential increase was 7.3 m (notice increase in water content at that depth).

		4/7/2009	5/4/2010				
Depth of increase (m)	Depth, m	θ	θ				
7.3		Day 1	Day 393	s1	s2	ΔS -below ZFP	ΔS -above ZFP
	0.5	0.3716	0.3708	0.1858	0.1854	-0.0004	
	1.5	0.3726	0.3734	0.3721	0.3721	0.0000	
	2.5	0.3781	0.3797	0.3754	0.3766	0.0012	
	3.5	0.2220	0.2497	0.3001	0.3147	0.0147	
	5.0	0.1676	0.1611	0.2922	0.3081	0.0159	
	7.3	0.2880	0.2938	0.5239	0.5231	-0.0008	
	9.7	0.2907	0.2904	0.6944	0.7010	0.0066	
	Storage Increase (m)	PREC (m)	HARG (m)	COMBO (m)			
	0.0363	0.0945	0.0040	0.0134			
Percent Difference			88.99	63.13			
(Precipitation-ET)- ΔS		0.0582	-0.0323	-0.0229			

Table 19) CNG front #4-Precipitation and ET estimates used for available storage for comparison.

HARG (Hargreaves and Samani, 1982)							
Date	prec (mm)	sum (mm)	sum (m)	ET (mm)	Prec-ET (mm)	sum (mm)	sum (m)
200902	10.4140			24.4795	-		
200903	23.6220			33.4701	-9.8481		
200904	42.9260	76.9620	0.0770	38.9195	4.0065	4.0065	0.0040
200905	17.5260	94.4880	0.0945	60.7346	43.2086		0.0040
COMBO (Szilagyi and Jozsa (2009) plus Dugan and Zelt (2000))							
Date	ET (mm)	Prec-ET (mm)	sum (mm)	sum (m)			
200902	0.0000	10.4140					
200903	20.5900	3.0320					
200904	84.6300	-41.7040	13.4460	0.0134			
200905	115.3400	-97.8140		0.0134			

Table 20) CNG front #5 reached a depth of 2.5 m resulting in an increase in storage beyond 2.5 m.

		10/27/2009	5/27/2010				
Depth of increase (m)	Depth, m	θ	θ				
2.5		Day 1	Day 212	s1	s2	ΔS -below ZFP	ΔS -above ZFP
	0.5	0.2950	0.3697	0.1475	0.1849	0.0374	
	1.5	0.2649	0.3724	0.2800	0.3711	0.0911	
	2.5	0.3547	0.3807	0.3098	0.3766	0.0668	
	3.5	0.2543	0.2426	0.3045	0.3117	0.0071	
	5.0	0.1531	0.1585	0.3056	0.3008	-0.0047	
	7.3	0.2801	0.2819	0.4982	0.5065	0.0083	
	9.7	0.2901	0.2899	0.6842	0.6862	0.0019	previous event
	Storage Increase (m)	PREC (m)	HARG (m)	COMBO (m)			
	0.2024	0.3119	0.1071	0.1186			
Percent Difference			47.07	41.39			
(Precipitation-ET)- ΔS		0.1096	-0.0952	-0.0837			

Table 21) CNG front #5 available precipitation and ET estimates.

HARG (Hargreaves and Samani, 1982)							
Date	prec	sum (mm)	sum (m)	ET (mm)	prec-ET (mm)	sum (mm)	sum (m)
200908	41.9100			70.6215	-		
200909	18.0340			44.4154	-		
200910	96.7740			20.3813	76.3927		
200911	10.4140			17.7795	-7.3655		
200912	2.2860			8.9354	-6.6494		
201001	16.7640			10.6941	6.0699		
201002	24.3840			11.3264	13.0576		
201003	37.0840	247.6500	0.2477	25.5008	11.5832	107.1034	0.1071
201004	22.0980	269.7480	0.2697	45.6600	-		
201005	42.1640	311.9120	0.3119	58.1180	15.9540	107.1034	0.1071
COMBO (Szilagyi and Jozsa (2009) plus Dugan and Zelt (2000))							
Date	ET	prec-ET	sum mm	sum m			
200908	93.6600	-51.7500					
200909	57.7900	-39.7560					
200910	11.4800	85.2940					
200911	0.0000	10.4140					
200912	0.0000	2.2860					
201001	0.0000	16.7640					

201002	20.5900	3.7940					
201003	84.6300	-47.5460	118.5520	0.1186			
201004	115.3400	-93.2420					
201005	157.6100	-	118.5520	0.1186			

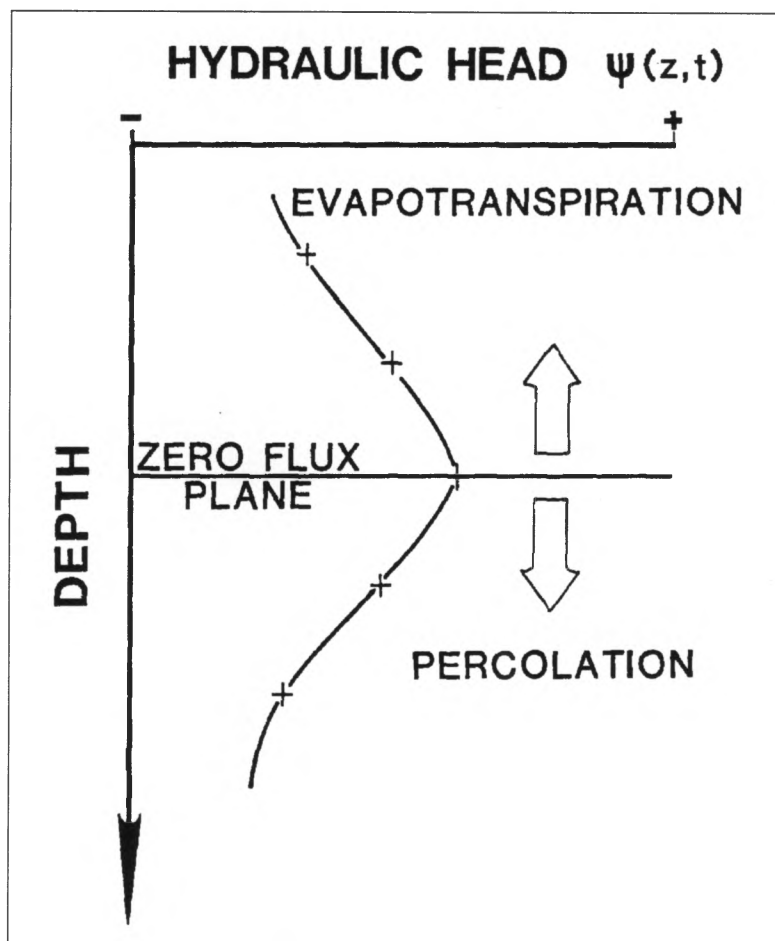


Figure 1. Simplified diagram of zero-flux plane concept showing fluid movement from high hydraulic head to low hydraulic head. (modified from *Dreiss and Anderson*, [1985])

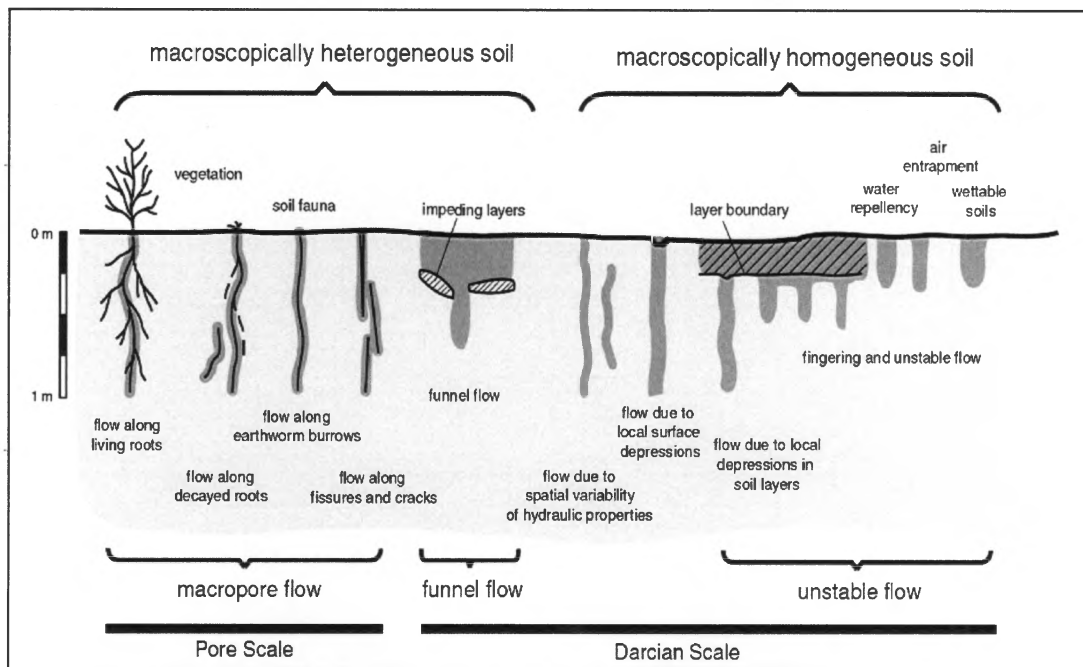


Figure 2. Mechanisms of preferential flow at different spatial scales (modified from Hendrickx and Flury [2001])



Figure 3. Water-repellent sandy soil of the High Plains aquifer
(Photo by Jason Gurdak)

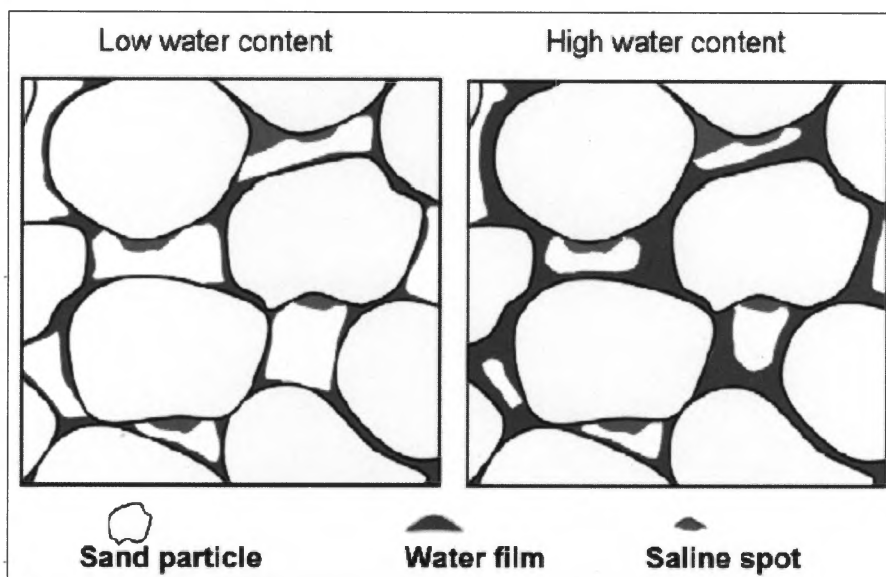


Figure 4. Conceptual model of pore-scale dual-domain flow (modified from Rimon et al., [2011])

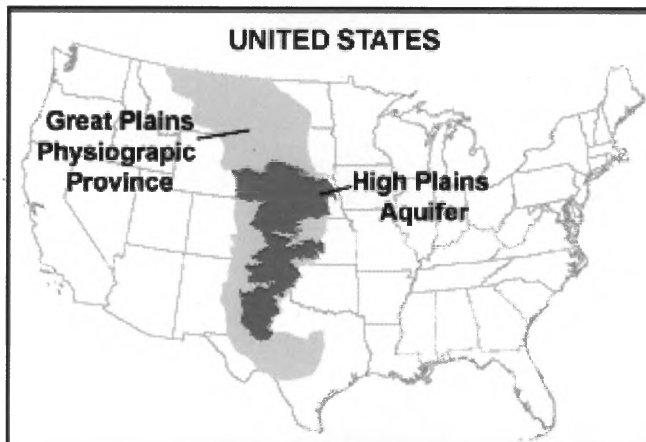


Figure 5. Great Plains physiographic province with an outline of the High Plains aquifer (modified from ne.water.usgs.gov, 2011)